International Journal of Biological Macromolecules 253 (2023) 127247

Contents lists available at ScienceDirect

International Journal of Biological Macromolecules

journal homepage: www.elsevier.com/locate/ijbiomac

Bacteriophage entrapped chitosan microgel for the treatment of biofilm-mediated polybacterial infection in burn wounds

Deepa Dehari [a], Dulla Naveen Kumar [a], Aiswarya Chaudhuri [a], Akshay Kumar [b], Rajesh Kumar [b], Dinesh Kumar [a], Sanjay Singh [c], Gopal Nath [b], Ashish Kumar Agrawal [a,*]

[a] Department of Pharmaceutical Engineering and Technology, Indian Institute of Technology (BHU), Varanasi 221005, U.P., India
[b] Department of Microbiology, Institute of Medial Science, Banaras Hindu University, Varanasi 221005, U.P., India
[c] Babasaheb Bhimrao Ambedkar University, Lucknow 226025, U.P., India

ARTICLE INFO

Keywords:
Bacteriophage formulation
Microparticles
Polybacterial infections
Wound healing
Antibiotic resistance

ABSTRACT

Staphylococcus aureus (*S. aureus*) and *Pseudomonas aeruginosa* (*P. aeruginosa*) bacteria are most commonly present in burn wound infections. Multidrug resistance (MDR) and biofilm formation make it difficult to treat these infections. Bacteriophages (BPs) are proven as an effective therapy against MDR as well as biofilm-associated wound infections. In the present work, a naturally inspired bacteriophage cocktail loaded chitosan microparticles-laden topical gel has been developed for the effective treatment of these infections. Bacteriophages against MDR *S. aureus* (BPSAΦ1) and *P. aeruginosa* (BPPAΦ1) were isolated and loaded separately and in combination into the chitosan microparticles (BPSAΦ1-CHMPs, BPPAΦ1-CHMPs, and MBP-CHMPs), which were later incorporated into the SEPINEO™ P 600 gel (BPSAΦ1-CHMPs-gel, BPPAΦ1-CHMPs-gel, and MBP-CHMPs-gel). BPs were characterized for their morphology, lytic activity, burst size, and hemocompatibility, and BPs belongs to *Caudoviricetes* class. Furthermore, BPSAΦ1-CHMPs, BPPAΦ1-CHMPs, and MBP-CHMPs had an average particle size of 1.19 ± 0.11, 1.42 ± 0.21, and 2.84 ± 0.28 μm, respectively, and expressed promising *in vitro* antibiofilm eradication potency. The ultrasound and photoacoustic imaging in infected burn wounds demonstrated improved wound healing reduced inflammation and increased oxygen saturation following treatment with BPs formulations. The obtained results suggested that the incorporation of the BPs in the MP-gel protected the BPs, sustained the BPs release, and improved the antibacterial activity.

1. Introduction

Antimicrobial Resistance (AMR) is one of the raising challenges that occurs when bacteria, viruses, fungi, and parasites no longer respond to medicines. According to the Antibiotic Resistance Threat Report-2019, about 2.8 million infections with antibiotic-resistant microbes occur in the USA each year, resulting in >35,000 deaths [1]. Among the different infections, burn wound infections are the 4th most common infections after falls, physical violence, and traffic accidents [1,2]. As per the World Health Organisation, approximately 3,00,000 fatalities occur due to burns each year, with addition mortality associated with heat and other causes of burns, including electric devices, radioactive radiation, chemical substances, *etc.* *Staphylococcus aureus* (*S. aureus*) and *Pseudomonas aeruginosa* (*P. aeruginosa*) are most frequently present in burn wound infections [3,4]. Furthermore, biofilms are typically found in the majority of wounds, consisting of various bacterial species, thereby contributing to prolonged delays in the wound-healing process [3,5,6]. Although bacteriophage (BP) has been proven to be effective against MDR bacterial infections, maintaining the BP titer in the formulation. Further, unavailability of regulatory and kinetic profile data, and controlling the release from the formulation are the major challenges for bacteriophage (BP) therapy. Additionally, maintaining bacteriophage biological stability (lytic activity) due to environmental conditions (during processing, formulation development, or at the site of application) is difficult.

Following the consideration of the obstacles, we have successfully formulated a gel containing BP-loaded chitosan microparticles to effectively address the issue of multidrug-resistant biofilm-induced bacterial infections in burn wounds. Chitosan, a biopolymer derived from crustaceans, is biocompatible, nontoxic, and has shown promise in scientific studies for its potential antimicrobial properties [7,8]. Chitosan's versatility makes it suitable for wound dressings, delivery systems,

* Corresponding author at: Department of Pharmaceutical Engineering and Technology, Indian Institute of Technology (BHU), Varanasi 221005, India.
E-mail address: ashish.phe@iitbhu.ac.in (A.K. Agrawal).

https://doi.org/10.1016/j.ijbiomac.2023.127247
Received 1 May 2023; Received in revised form 19 September 2023; Accepted 2 October 2023
Available online 5 October 2023

and as a biomaterial for encapsulating bacteriophages (BPs), as demonstrated in prior publications [9–14]. Some grades of chitosan with low deacetylation may have limited water solubility, necessitating 0.1–2 % acetic acid or formic acid for solubilization, which can be detrimental to bacteriophage survival. In the present work, we have used chitosan (chitosan oligosaccharide, water-soluble grade, extra pure, >90 % degree of deacetylation), which is biodegradable, biocompatible, and non-toxic with the potential for pharmaceutical applications and bacteriophage encapsulation [15]. Microparticles offer severals advantages over nanoparticles as bacteriophage carriers. Their larger size simplifies preparation, handling, and characterization, enabling controlled and sustained release for prolonged therapeutic effects, while also protecting the active pharmaceutical ingredients [16,17].

Further, we used trehalose to protect the bacteriophage viral capsid from thermal stress and desiccation. Trehalose restores the conformational and structural stability of BP through hydrogen bonding or vitrification, reducing protein mobility [18]. Additionally, water-soluble grade chitosan oligosaccharide and SEPINEO™ P 600 (the polymer acts as a thickener, an emulsifier, and a stabilizer all in one) further improve the applicability, texture, and stability, of the final formulation. As far as our current knowledge goes, this represents the first comprehensive report on the usage of BPs against bacterial infections caused by multiple species (*S. aureus* and *P. aeruginosa*). Furthermore, we utilized advanced imaging techniques, including photoacoustic and ultrasound imaging instrument, to evaluate wound healing. The developed bacteriophage formulation was characterized further by several *in vitro* and *in vivo* studies to establish the efficacy against MDR bacterial infections.

2. Materials and methods

2.1. Materials

Muller Hinton Agar (MHA), TMG buffer (Tris hydrochloride, magnesium sulfate, gelatine), Agar (bacteriological grade), Luria Bertini (LB), antibiotics discs, and pure drugs (Colistin and Vancomycin) were purchased from Himedia laboratories, Maharashtra, India. Chitosan (extra pure, water-soluble, molecular weight < 3000 and degree of deacetylation ≥90 %), trehalose dihydrate, and STPP (sodium tripolyphosphate) were acquired from Sisco Research Laboratories, Mumbai, India. Filmtracer® Live/Dead Biofilm Viability Kit and DiD (DiIC18(5); 1,1′-dioctadecyl-3,3,3′,3′- tetramethylindodicarbocyanine, 4-chlorobenzenesulfonate salt) were bought from, Thermo Fisher, Waltham, USA. Dulbecco's Modified Eagle Medium (DMEM) media (Himedia Laboratories, Mumbai, India), Fetal Bovine Serum FBS (Sigma Aldrich, Bangalore, India), and Triton® X-100 (Sigma Aldrich, Bangalore, India) used during the experiments were of molecular grade. All other chemicals and reagents used in this study were bacteriological and laboratory-grade.

2.2. Methods

2.2.1. Bacterial stain collection

S. aureus (BHU/SA/4193) and *P. aeruginosa* (BHU/PA/1956) bacteria were collected from a patient pus sample of a wound, under supervision of Professor Gopal Nath, Department of Medical Microbiology, IMS, BHU, Varanasi, India. The obtained bacterial samples were sub-cultured in MacConkey and blood agar media at 37 °C overnight. Moreover, the bacterial strains were retained on nutrient agar slants at a temperature of 4 ± 1 °C until they were to be utilized in subsequent experiments.

2.2.2. Antibiotic sensitivity test

In this study, antibiotic discs (Fig. S1, Tables S1 and S2), pure colistin, and vancomycin were used to test the antibiotic sensitivity of bacterial strains using the Kirby-Bauer technique. Briefly, antibiotic disks were placed in bacterial lawned Muller-Hinton agar plates and overnight incubated at 37 °C. Muller-Hinton agar has the advantage of allowing antibiotics to diffuse better than most other media. Inhibition zones are more accurate when diffusion is better [19]. In addition, the antimicrobial agents colistin (at concentrations ranging from 0.1 to 5 μg/mL) and vancomycin (at concentrations ranging from 0.1 to 5 μg/mL) were subjected to testing against *P. aeruginosa* and *S. aureus*, respectively. This testing was conducted using the standard broth microdilution approach as outlined by the guidelines set forth by the Clinical and Laboratory Standards Institute (CLSI) [20–22]. Based on the CLSI guidelines, colistin MICs are ≤2 (susceptible) and >2 mg/L (resistant), whereas vancomycin MICs are ≤1.5 (susceptible) and >2 mg/L (resistant Moreover, bacterial isolates are classified as MDR (multidrug-resistant) when they exhibit resistance to a minimum of one agent in three or more classes of antimicrobial drugs. In this experiment, *P. aeruginosa* ATCC 27853 strain and *S. aureus* ATCC 25923 strains were taken as controls.

2.2.3. Bacteriophage isolation, amplification, and purification

The BPs targeting the MDR bacteria *P. aeruginosa* and *S. aureus* have been isolated from water samples collected from the Ganges River and the sewage water of Sunder Lal Hospital (BHU). The collected water samples were centrifuged at 9408 ×g (REMI NEYA C-24 plus, India) for 15 min at 4 °C, and supernatants were collected. The process was repeated thrice to remove settled bacteria and debris. After that, a filter with a pore size of 0.45 μm was used to filter the supernatants. Further, processed water samples were dropped in a separate lawned bacterial MHA plate and overnight incubated at 37 ± 1 °C. Following the incubation period, the petri plates were determined for the appearance of plaques and subsequently harvested using TMG buffer. The process of culturing and harvesting was iterated until achieving complete bacterial clearance, which was associated with a higher BP titer [23,24].

The BP concentration was enhanced by amplification, which included three steps; firstly, the isolated BPs were dropped on lawned bacteria in a small Petri plate (60 mm) and incubated at 37 °C for 16–18 h, and harvested. This process was repeated until complete bacterial clearance of the entire plate was obtained. Secondly, the procedure followed in step 1 was scaled up using a bigger size petri dish (140 mm). Finally, BP concentration was amplified using a culture Roux bottle (255 × 120 mm). The foreign materials (bacteria, agar media, endotoxin, *etc.*) were separated from BP by 0.22 μm syringe filtration followed by polyethylene glycol (PEG) purification method [25].

2.2.3.1. Quantification of bacteriophage with plaque morphology. The quantification of BPs was conducted using the double-layer agar overlay (DLAO) method, and the results were expressed as the BP titer value PFU/mL. Briefly, 200 μL of bacterial host and 1 mL BP Solution were mixed in soft agar (0.8 % agar) in a molten state. The suspension of BP and host was overlaid with bottom solid agar petri plates. The plates were gently swirled, allowed to dry at ambient temperature for 10 min, and subsequently incubated overnight at a temperature of 37 °C. On the next day, the BP titer was quantified using the following equation [26].

$$\text{Bacteriophage titer (PFU/ml)} = \frac{\text{Numberof plaques per ml}}{\text{Dilution factor}}$$

Plaques from the DLAO test were examined for plaque size, halo zones surrounding plaques, and rate of bacterial clearance [27,28]. The experiment was repeated thrice to determine the average plaques.

2.2.3.2. Morphological evaluation of bacteriophage. In order to categorize BPs according to their size, shape, and morphology transmission electron microscopy (TALOS Cryo-TEM, Thermo scientific at SAIF-AIIMS Delhi) was utilized The BPs suspension (13.6 mL, approximately 10^9–10^{10} PFU/mL) were subjected to centrifugation at 30,000 ×g for 60 min. The resulting pellet was then washed three times using

0.1 M ammonium acetate (13.6 mL, pH 7.0). Subsequently, the pellet was reconstituted in a solution of 200 μL ammonium acetate. The prepared samples, measuring 5 μL, were applied onto a carbon coated TEM grid. Afterward, negative staining was performed using 5 μL of phosphotungstic acid [29]. The average size of three TEM images of phages was used to measure the size of BPs.

2.2.3.3. Bacteriophage lytic range with phagogram. The BP lytic range (host specificity) was determined by using a modified phagogram spot test [6,30] and verified by using the DLAO method on 46 bacterial isolates, which have been mentioned in Table S3. In brief, 5 μL (10× serially diluted) of BPs (BPSAΦ1 and BPPAΦ1) were dropped serially from high to low concentration on separate dry petri plates (90 mm, diameter) containing 0.8 % w/v soft agar combined with 200 μL (1 OD) of individual bacterial species followed by overnight incubation at 37 °C. The following day, petri plates were visually examined for a clear spot. The lysis activity was confirmed by performing the DLAO method of lowest lytic active dilution and observed for the plaques. Each spot test was performed in triplicate.

2.2.3.4. Adsorption rate assay. Aliquots of BPs were incubated (37 °C) with host strain cultures at the MOI (0.01). At 0, 3, 6, 9, 12, 15, and 18 min, samples (100 μL) were collected and centrifuged to separate the bacterial cells. At each time interval, the supernatants were titrated for the detection of unabsorbed BPs [31].

2.2.3.5. Singular step growth curve. To assess the growth cycle of BPs in bacterial hosts (*S. aureus* and *P. aeruginosa*), a single-step growth curve was used. This study aids in estimating the latent period and burst size of phages BPSAΦ1 and BPPAΦ1. The standard approach, described by Ellis E.L. and Delbruck M., was used to calculate the one-step growth curve [32,33]. In brief, 8×10^6 CFU/mL of *S. aureus* and 2×10^6 CFU/mL of *P. aeruginosa* were centrifuged at 6000 ×g for 10 min and bacterial pellets were combined with 10 mL of BPSAΦ1 and BPPAΦ1, respectively. The bacteria were incubated at 37 °C with moderate agitation (150 rpm) and a multiplicity of infection (MOI) of 0.01. Centrifugation at 10,000 ×g for 5 min was used to eliminate any non-adsorbed BPs. The pellet was resuspended in 10 mL of LB media and put in an incubator. At the time interval of 5 min (5–70 min), 100 μL of bacteria-adsorbed-BP complex were collected. The sample set was diluted right away and put on a plate for a DLAO technique for BP titer measurement. The Experiment was conducted in triplicate. GraphPad Prism 5.0 was used to plot the time series data, and the sigmoidal curves were used to figure out the average burst size per infected host and the average latent period.

2.2.3.6. pH, temperature, and UV light stability studies of bacteriophage. To determine the pH stability, LB broth was prepared at different pH ranges (1.5, 3.5, 6.8, 7.4, and 8.5) with 6 M NaOH and HCl solution. BP suspension (1 mL) was added to each tube corresponding to each pH value and incubated at 37 °C for 24 h. To determine the thermal stability of the BP, 1 mL of its filtrate was incubated for 60 min at various temperatures (37, 50, 55, 60, 65, and 70 °C). The UV sensitivity of the BPs was tested by placing the 1 mL solution under a UV-C germicidal lamp (UV T8/25W, 253.7 nm, Philips, Ved group, India) for the specified duration (0, 5, 10, 15, and 20 min). The BP titer was determined after the experiment using the DLAO technique. The Experiment was conducted in triplicate [34–36].

2.2.3.7. Hemocompatibility assay of bacteriophages. Hemocompatibility testing is an important study to predict the possible biocompatibility of any material. The hemocompatibility assay of BP was performed by a previously reported method with slight modifications [37].

The human blood sample was obtained from the blood bank, collected in an EDTA tube, and centrifuged at 135 ×g for 15 min to separate RBCs. The settled RBCs were washed thrice with PBS (pH 7.4), and a 2 % suspension of RBCs was prepared in PBS (pH 7.4). Further, 100 μL (~10^4 PFU/mL) of each sample (BPSAΦ1 and BPPAΦ1) were mixed separately, with 500 μL of prepared 2 % RBCs suspension and incubated at 37 °C for 1.5 h with gentle shaking at every 15 min. Further, each tube was centrifuged (212 ×g for 5 min), the supernatant (200 μL) was placed in 96 well plates, and the absorbance was recorded at a wavelength of 545 nm. The PBS (pH 7.4) and Triton™ X-100 (1 % v/v) treated RBCs samples were used as the negative and positive control groups, respectively. The experiment was repeated three times under the same conditions. The following method was used to figure out the hemolysis ratio (HR%);

$$\text{Hemolysis ratio percentage (HR\%)} = \frac{(\text{At} - \text{Anc})}{(\text{Apc} - \text{Anc})} * 100$$

The variables At, Anc, and Apc represent the absorbance values of the test samples, negative control, and positive control, respectively.

According to the American Society of Testing and Materials (ASTM, 2000), biomaterials are divided into three broad categories based on the degree of hemolysis, *i.e.* (a) hemolytic if hemolysis (%) is >5 %, (b) slightly hemolytic if hemolysis (%) is between 2 and 5 %, (c) non-hemolytic if hemolysis (%) is <2 %. Additionally, the hemolysis was qualitatively confirmed by microscope visualization following the Leishman stanning technique [38].

2.2.4. Formulation and characterization

To ensure the suitability of excipients (chitosan, sodium tripolyphosphate, trehalose, and glycerol) for formulation development, a compatibility assessment with BPs was conducted. The experimental procedure involved incubating BPs in LB (LB broth is a rich nutrient medium, originally developed for bacteriophage studies [39]) broth at 37 °C for 24 h, with each excipient at a 1:1 ratio. The determination of the BP titer was conducted utilizing the DLAO method [40].

2.2.4.1. Bacteriophage microparticle preparation. Chitosan microparticles (CHMPs) containing BPSAΦ1 (BPSAΦ1-CHMPs), BPPAΦ1 (BPPAΦ1-CHMP), and a combination of both BPs (MBP-CHMPs) were prepared using the ionic gelation technique. For the preparation of blank CHMPs, 650 mg of chitosan and 0.5 % w/v of D (+)-Trehalose dihydrate were dissolved in 50 mL of PBS and filtered through a 0.45 μm filter. The aqueous solution of sodium tripolyphosphate (STPP, 12 mg) was injected (gauge 28) dropwise into the solution under sterile conditions, with constant magnetic stirring at a rate of 200 rpm, and at 25 °C. Separately, 1.0 mL of the BP suspension (BPSAΦ1 or BPPAΦ1 or both mixed bacteriophage (MBP)) was added to the polymeric solution, and similarly, STPP solution was added dropwise with continuous stirring to get the BP-loaded CHMPs. To clean the pellets from the microparticles (MPs), they were centrifuged at 3387 ×g for 10 min, and then given two washes with PBS (3 mL) and lyophilized [11,41]. The composition of the

Table 1
Composition of the various microparticle formulations.

Group	Chitosan (mg)	BPSAΦ1 (PFU/mL)	Trehalose % (w/v)	BPPAΦ1 (PFU/mL)	STPP (mg)
Blank CHMPs	650	–	0.5	–	12.0
BPSAΦ1-CHMPs	650	4E+09	0.5	–	12.0
BPPAΦ1-CHMPs	650	–	0.5	1.3E+04	12.0
MBP-CHMPs	650	4E+09	0.5	1.3E+04	12.0

Blank CHMPs: Blank chitosan microparticles.
BPSAΦ1-CHMPs: Bacteriophage against *S. aureus* chitosan microparticles.
BPPAΦ1-CHMPs: Bacteriophage against *P. aeruginosa* chitosan microparticles.
MBP-CHMPs: Mixed bacteriophage chitosan microparticles.

various CHMPs has been presented in Table 1.

2.2.4.2. Microparticle incorporation into gel. The prepared microparticles have been incorporated into the gel and applied topically to the burn site. The microparticle-containing gel was made in a laminar-flow aseptic environment. In brief, 5 mL of filtered SEPINEO™ P600 (2.5 % v/v of total formulation), 1 g of lyophilized MBP-CHMPs, and 0.5 % of sterilized glycerol were stirred at 200 rpm during 30 min to generate a homogeneous gel. The gel was combined with BP microparticles, and after resting overnight to allow for adequate swelling, it was named as MBP-CHMPs gel [42]. The blank gel was formulated without incorporating MPs while the BPSAΦ1-CHMPs and BPPAΦ1-CHMP laden gel were prepared by using the above method with the incorporation of 1.0 g of the individual MPs.

2.2.4.3. Analysis of particle size, polydispersity index, and zeta potential. The zetasizer (Nanoseries Malvern Zetasizer, S90) was used to measure the particle size (PS), polydispersity index (PDI), and zeta potential (ZP) of the developed MPs by electrophoretic mobility and dynamic light scattering technique. Microdispersion dilutions of 0.1 mL to 1 mL were used to dilute samples in Millipore water for the analysis [43].

2.2.4.4. Determination of entrapment efficiency. The indirect method was used to calculate entrapment efficiency (EE%) of BP in MPs. The MPs were separated by centrifuging the mixture at 4 °C and 21,168 ×g for 15 min. After collecting the supernatant, it was diluted serially [44]. The DLAO technique was used to quantify the BP concentration in the supernatant. Experiments were performed in triplicate. The following equation was used to calculate the entrapment efficiency (EE%).

$$EE\% = \frac{\text{Total amount of incorporated BP} - \text{free BP}}{\text{Total amount of incorporated BP}} \times 100$$

2.2.4.5. MBP-CHMPs-gel characteristics. The organoleptic characteristics, including clarity and odor, as well as the homogeneity of the gel, were assessed through visual examination. The viscosity of the BP-CHMPs-gel sample was determined using a Brookfield viscometer DVE with LV Spindle no. 61. The viscometer spindle was immersed in a beaker containing 20 g of gel and rotated at a speed of 50 rpm at ambient temperature. The viscosity of the samples was measured and recorded in centipoise units [45]. Furthermore, the gel that was prepared underwent screening through the utilization of a spreadability test. In a concise manner, a quantity of 0.5 g of the gel was carefully transferred onto a glass palate that had been previously marked with a circle measuring 2 cm in diameter. The spreadability of the gel was subsequently assessed by applying a second glass plate on the upper surface, subjecting it to a weight of 500 g for 5 min. The diameter of the circle was measured as it expanded following the dispersion of the gel [46]. Every measurement was performed three times, with a fresh sample each time.

2.2.4.6. In vitro release study. The dialysis bag method was employed to conduct *in vitro* release studies of MPs loaded with BPSAΦ1 and BPPAΦ1, as well as MPs laden gel [47]. In this experiment, formulations were introduced into a glass beaker containing 100 mL of PBS with a pH of 7.4. The entire setup was kept at a temperature of 37 °C and stirred constantly at a rate of 50 rpm. At times, samples with a volume of 1 mL were extracted for analysis. To ensure that the sink conditions were maintained, the extracted samples were replaced with an equal volume of fresh medium. The quantity of BP that was released, assessed through the utilization of the DLAO methodology. The *in vitro* release studies were performed in triplicate for each BP sample. To determine the release kinetics, the data from the *in vitro* release were fitted to different models [48,49].

2.2.4.7. Surface morphology. Scanning electron microscopy (SEM; Evo-Sem, Carl Zeiss Microscopy Ltd.) was used to assess the surface morphologies of the prepared MBP-CHMPs, MBP-CHMPs-Gel, and blank gel. A single droplet of MPs, diluted by a factor of 50, was applied onto a coverslip. The droplet was evenly distributed and allowed to dry overnight under a vacuum. Subsequently, a layer of carbon was applied to the dried sample, and it was imaged using SEM. The imaging procedure involved utilizing a lyophilized sample of gel containing MPs, employing the same methodology [47].

2.2.5. In vitro antibacterial studies

2.2.5.1. Spot test. The qualitative assessment of BPSAΦ1-CHMPs, BPPAΦ1-CHMPs, MBP-CHMPs, blank CHMPs, blank gel, and MBP-CHMPs-Gel was conducted using a drop test method against *S. aureus* and *P. aeruginosa* bacteria. In brief, a volume of 20 μL from each sample (performed in triplicate) was applied onto a bacterial lawned MHA plate with a density of 0.5 McFarland units. The plates were then incubated at a temperature of 37 °C for the duration of one night. Following the incubation period, the activity of the samples was assessed through the observation and measurement of the clear zone.

2.2.5.2. Minimum inhibitory concentration & minimum bactericidal concentration. The minimum inhibitory concentration (MIC) determined for three distinct groups, namely BPSAΦ1-CHMPs, BPPAΦ1-CHMPs, and MBP-CHMPs, were assessed following the guidelines established by the CLSI. This evaluation was conducted on planktonic cultures of the host organisms *S. aureus* and *P. aeruginosa*, utilizing the microbroth dilution method. In brief, *S. aureus*, *P. aeruginosa*, and a combination of both bacterial strains were cultured individually in LB broth at a concentration of 2.3×10^8 CFU/mL. Subsequently, a series of dilutions were performed on 100 μL of MPs (specifically BPSAΦ1-CHMPs, BPPAΦ1-CHMPs, and MBP-CHMPs) with concentrations ranging from 0.1 to 10 mg/mL. These diluted samples were then added to individual wells. The experimental setup included the maintenance of corresponding bacterial controls, which consisted of bacteria grown in LB medium. Controls for the corresponding bacteria (bacteria cultured in LB broth), bacteriophages (BPs stock solution), and medium were maintained. Microtiter plates were incubated for 37 °C for 24 h while being gently shaken at a rate of 20 rpm. The MIC was determined to be the lowest concentration of BP at which there was no evidence of turbidity [47].

The CLSI procedure was also used to determine the minimum bactericidal concentration (MBC). After 24 h of growth at 37 °C, no visible growth was seen in the wells of microplates, consequently, a sample (100 μL) was collected from those wells and put on the top of MHA plates. The sample was kept at 37 °C for a full 24 h. MBC stands for the minimum concentration of the drug at which no colonies formed. The absence of growth on the MHA plate meant that the concentration was lower than the 10 CFU/mL threshold used in this assay [50]. Experiments were repeated three times.

2.2.5.3. Antibiofilm assay. The capacity of BPs to eradicate established biofilms and the ability to prevent biofilm development was determined using antibiofilm assay. The antibiofilm effectiveness of BPSAΦ1-CHMPs, BPPAΦ1-CHMPs, and MBP-CHMPs was evaluated using a crystal violet quantitative microtiter plate test [51,52]. In short, 180 μL of LB growth medium containing 20 μL of bacteria (*S. aureus* and, 0.5 OD600nm) were transferred (separately and in combination (10 + 10 L)) in a sterile microtiter plate and incubated (37 °C) for 48 h. Furthermore, planktonic bacteria were removed out, and 200 μL (2× MIC) of MPs were added to each well. The wells were then left to incubate for 24 h. After incubation, the sample was taken out of the microplate wells and washed extensively with PBS (pH 7.4) to get rid of free floating bacteria that hadn't adhered to the surface. The microplate were then allowed to air-dry for 60 min. After drying, adhered "sessile" bacteria in the plates had been fixed with sodium acetate (2 % w/v),

then submerged with crystal violet (1 % w/v) dye and left in a dark environment for 30 min. The leftover color was carefully removed from the wells using deionized water and dried. After the plate had dried, 200 μL of 95 %, v/v ethyl alcohol was added to each well. A multiscan plate reader (Thermo Fisher Scientific) was used to measure the absorbance (620 nm). Control wells contained only growth media inoculated with the tested bacterial isolates. The mean of the three measurements has been reported. The percentage of inhibition of biofilm formation was calculated using the following equation.

$$\text{Inhibition}\% = \frac{\text{Optical density of control} - \text{Optical density of treatment}}{\text{Optical density of control}} * 100$$

Further the biofilm formation prevention were determined by incubation of bacteria, formulations in LB growth media incubated for 48 h and checked the biofilm formation with compare to control biofilm.

2.2.5.4. Microscopy of biofilm. The overnight cultures of *S. aureus, P. aeruginosa*, and a blend of both bacteria were distributed into a 12-well culture plate equipped with sterile round coverslips. Subsequently, the plate was placed in an incubator and left undisturbed for a period of 48 h. After incubation, the formed biofilm was treated with BPSAΦ1-CHMPs, BPPAΦ1-CHMPs, and MBP-CHMPs in a concentration of ($\sim 10^9$ PFU/mL) and then incubated further for 24 h. Next, the glass slide was washed by using PBS, and Filmtracer Live/Dead Biofilm Viability Kit was used for staining cells inside the extracellular matrix. Glass slides were submerged in SYTO9 (6 μM) and propidium iodide (30 μM) staining solution for 30 min. After staining, the glass discs were washed with PBS, and images were captured by confocal microscope (CLSM 900, Carl Zeiss Microscopy GMBH) at 40× magnification [53]. Further, the eradication of polybacterial biofilm was confirmed by SEM (Carl Zeiss Microscopy Ltd.) and Atomic Force Microscopy (AFM, NTEGRA Prima, NT-MDT) [54].

2.2.5.5. Cytotoxicity study. The methylthiazolyldiphenyl-tetrazolium bromide (MTT) assay was used to assess the safety and impact of chitosan microparticle formulations and BP treatment on the viability of HEK-293 cells [55,56]. HEK-293 cell lines were graciously donated by Prof. Subash Chandra Gupta, Department of Biochemistry, Institute of Science, Banaras Hindu University. Cells were cultured in DMEM medium with 10 % FBS and 1 % penicillin-streptomycin at 37 °C in a humidified chamber. Briefly, cells were seeded in a 96-well plate at the density of 1×10^5 cells per well and incubated for 24 h for cell attachment. Further, media was aspirated, fresh media containing different bacteriophage formulations (BPSAΦ1-CHMPs, BPPAΦ1-CHMPs, and MBP-CHMPs), as well as pure BP at a level of 10^5 PFU/mL, was added, and incubated for 24 h. Additionally, PBS (pH 7.4) was used as a negative control, and 1 % triton X-100 was used as a positive control. Following the completion of the incubation period, the media was aspirated and replaced with the fresh media containing MTT (0.5 mg/mL) followed by further incubation for 4 h. After incubation, this media was discarded and DMSO (100 μL) was added to dissolve the insoluble formazan crystals. A spectrophotometer was used to measure cell viability at 580 nm (Multiskan™ FC Thermo Fisher Scientific, India). Experiments were repeated three times. The toxicity caused by formulations and bacteriophages was measured in terms of percentage cell viability parameters.

2.2.6. In vivo studies

Female/male Wistar rats (200–250 g) were used for the study and all the animal experiments conducted in this study received ethical approval from the Institutional Animal Ethics Committee (IAEC), IIT BHU, Varanasi, Uttar Pradesh, India. The animals were randomly assigned to five groups, with each group consisting of five animals (n = 5).

2.2.6.1. In vivo wound healing study with USG/PA monitoring. Rats were administered intraperitoneal ketamine (80 mg/Kg) and xylazine (20 mg/kg) for anesthesia induction before developing the burn wound. A stainless-steel rod with a cylindrical shape and a diameter of 1.5 cm was heated to a temperature of 100 °C by immersing it in boiling water. Subsequently, the heated rod was carefully positioned on the dorsal region of the rat for a duration of 20 s. After 6 h of wound creation, *S. aureus* bacterial dispersion (100 μL; 1 OD), *P. aeruginosa* bacterial dispersion (100 μL; 1 OD), and a mixture of both the dispersions (100 μL; 1 OD; 1:1 ratio) was injected subcutaneously and swabbed on the wound area for continuous two days. This process was intended to induce a bacterial infection and promote the formation of a strong biofilm within the wound. Animals were randomly divided into five groups (n = 5); group 1: control group (without treatment), group 2: treatment with marketed formulation, Silvadene® cream (silver sulfadiazine, SSD 1.0 %), group 3: treatment with BPSAΦ1-CHMPs gel, group 4: treatment with BPPAΦ1-CHMPs gel, group 5: treatment with MBP-CHMPs gel. The therapeutic efficacy in promoting wound healing of the developed formulations was assessed by wound area reduction measured by a scale on different days until the completion of re-epithelialization. Simultaneously, the measurement of wound volume and oxygen saturation was conducted using an Ultrasound/Photoacoustic (USG/PA) imaging system (VisualSonics, Vevo F2 LAZR-X PA scanner, UHF 48 transducer) [57,58]. After the development of an infection, in each group, BP loaded formulation (500 mg) was applied twice daily, and wound healing was evaluated. Wound re-epithelialization was quantified using a scale; [percentage wound retraction on day X = (wound area on day zero - wound area on day X) / (wound area on day zero)], and angiogenesis was validated using USG/PA imaging. The length of time for re-epithelialization was calculated as the number of days needed for wound healing and for the eschar to come off, leaving no raw wound remaining.

Once the animal's wound had completely regenerated a new layer of epithelium, the skin at the wound site and highly vascular organs were carefully excised. These samples were then preserved in formalin for fixation. Subsequently, they underwent processing and embedding in paraffin to facilitate sectioning. Slices with a thickness of 5 μm were prepared and stained using the hematoxylin and eosin method for microscopic examination. The duration of re-epithelialization was determined by calculating the number of days required for complete wound healing and for the eschar to come off, leaving no raw wound remaining.

2.2.7. Gel occlusion and bioimaging study

MPs and gels loaded with DiD dye were formulated to enable fluorescence imaging of the wound area following their application. The Photon Imager Optima System (Biospace Lab, France) was employed for capturing the fluorescence images. The *in vivo* wound-healing animals were reused in this study, with three animals in each group. Animals were anesthetized under a continuous flow of 3 % isoflurane and fluorescence signals were captured at excitation and emission wavelengths of 620 and 710 nm, respectively at 0.5, 1, 2, 4, and 6 h post-application of the free DiD and DiD loaded formulation. The radiant efficiency (measured as fluorescence intensity/area/time) was analyzed using the Biospace Lab imaging software (M3Vision), and the region of interest (ROI) tool was used for circling the wound area.

2.2.8. Stability studies

BP suspension, BP microparticles, and BP microparticles gel were sealed and stored (in triplicate) at 4 °C for 8 months. At the end of each month, the samples were enclosed within a dialysis bag and maintained in 50 mL of sterile PBS (pH 7.4) for a period of 24 h, separately. Subsequently, the viability and ability to lyse host bacteria were evaluated using the DLAO [59].

2.2.9. Statiscal analysis

The experimental findings from both *in vitro* and *in vivo* studies were reported as the Mean ± SD, with a sample size of 3 (*in vitro*) and 5 (*in vivo*). Statistical analysis was performed using GraphPad Prism 5.0. One-way ANOVA and post Tukey's test was utilized to determine the level of statistical significance between groups. ns ($p \geq 0.05$), * ($p < 0.05$), ** ($p < 0.01$), and *** ($p < 0.001$) were considered statistically significant levels.

3. Results and discussions

3.1. Antibiotic sensitivity test

Susceptibility of the bacteria towards the antibiotics was performed by antibiotic susceptibility test. *S. aureus* demonstrated susceptibility (Fig. S1, Table S1) towards co-trimazole (30 μg), ampicillin (10 μg) + sulbactam (10 μg), cefepime (30 μg), linezolid (30 μg), clindamycin (2 μg), amikacin (30 μg), and vancomycin (MIC = 1.80 μg/mL) and resistance against ampicillin (10 μg), cefotaxime (30 μg), gentamycin (10 μg), penicillin (10 μg), erythromycin (15 μg), and ciprofloxacin (5 μg). Similarly, *P. aeruginosa* showed susceptibility towards (Fig. S1, Table S2) polymyxin B (300 unit), piperacillin + tazobactam (100 μg +10 μg), and colistin (MIC 1.5 μg/mL). However, *P. aeruginosa* demonstrated resistance to the antibiotics such as ofloxacin (5 μg), amikacin (10 μg), norfloxacin (10 μg), piperacillin (100 μg), ceftazidime (30 μg), gentamycin (10 μg), aztreonam (30 μg), cefepime (30 μg), imipenem (10 μg) and meropenem (10 μg) antibiotics. The obtained data suggested that both *S. aureus* and *P. aeruginosa* bacteria were resistant to multiple antibiotics and hence could be considered MDR strains. MDR *P. aeruginosa*-*S. aureus* co-infections have been reported to be more dangerous than single infections of either species [60].

3.2. Bacteriophage isolation, amplification, and purification

BPs were successfully isolated, amplified (~10^{12} pfu/mL quantified by DLAO) (Fig. 1A), and named as BPSAΦ1 (BP against *S. aureus*) and BPPAΦ1 (BP against *P. aeruginosa*).

3.2.1. Plaque assay

The plaque assay was used for growing isolated plaques of BP particles within a lawn of bacteria, and DLAO was used to quantify the grown BPs. The resultant plaque shows a clear, round shape, neat border with an average size of 1.03 ± 0.12 mm for *S. aureus* (Fig. 1A) and 4.8 ± 0.45 mm for *P. aeruginosa*.

Researchers reported, tiny, pinpoint plaques of BP (2 ± 0.23 mm) isolated against *S. aureus* and small, clear, round plaques of BP against *P. aeruginosa* with a diameter of approximately 2 ± 0.23 mm [61–63]. Additionally, it has been stated that Lytic BPs exhibit clear plaques, whereas lysogenic bacteriophages display turbid or bulls-eye plaques [64]. However, only molecular genome sequencing can assure the existence of lytic and lysogenic BP [65].

3.2.2. Morphological evaluation of bacteriophage

The morphological analysis of the BPs by TEM showed that BPSAΦ1 (Fig. 1B) has an icosahedral head capsid with a diameter of 88.9 nm, tail (115.2 nm long), and tail fibers, which is flexible with a full length of 201.1 nm. Similarly, BPPAΦ1 (Fig. 1D) TEM images showed an icosahedral head capsid (143.7 nm), long thin tail (193.7 nm), thin tail fibers, and flexible with full length up 337.3 nm. According to the latest guidelines set forth by the International Committee on Taxonomy of Viruses (ICTV), BPSAΦ1 and BPPAΦ1 have been assigned as members of the *Caudoviricetes* class.

3.2.3. Lytic range of bacteriophage

As per phagogram spot testing and confirmation by DLAO, it was noted that both BPSAΦ1and BPPAΦ1 depicted a limited host range, only impacting 10.86 % and 15.21 % of the 46 bacterial hosts (Table S3), respectively. Therefore, the available data indicated that both BPs are host-specific, making them the best candidates for personalized treatment. Commonly BPs are believed to infect only a small subset (narrow range) of closely related bacteria [66]. Biochemical interactions throughout infection, the existence of related prophages, and the

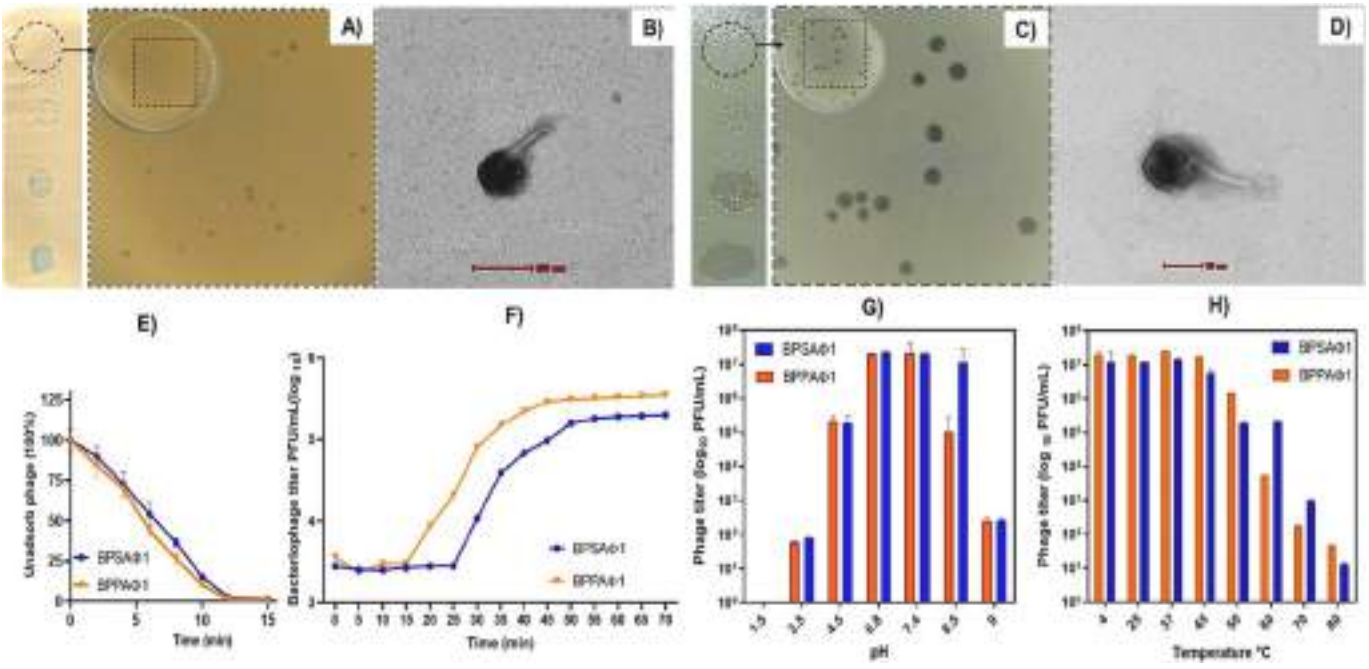

Fig. 1. Bacteriophage isolation and characterization, where (A) and (C) represents Bacteriophage plaques obtained by double layer agar overlay of *S. aureus* and *P. aeruginosa*; (B) and (D) represents the TEM image of BPSAΦ1 bacteriophage and BPPAΦ1 bacteriophage, respectively. Growth and lytic characterization, where (E) represents the absorption rate and (F) shows one-step growth curve of BPSAΦ1 and BPPAΦ1; (G) and (H) show a graphical representation of the pH and temperature stability of BPSAΦ1 and BPPAΦ1 BPs. Data for the release study has been presented as Mean ± SD (n = 3).

specificity of host receptor binding proteins for individual BPs are the common reasons for this observation [67]. However, certain isolated BPs have broad-spectrum action against *S. aureus* bacteria while having without affecting other bacterial strains [68].

3.2.4. Adsorption rate assay

A study was conducted to determine the rate of BP adsorption onto the surface of host bacteria using an adsorption assay. The graph obtained (Fig. 1E) illustrates the attachment of BPSAΦ1 and BPPAΦ1 to their respective host cells, *S. aureus and P. aeruginosa*. The data shows that approximately 50 % of the BPs were attached to the host cells within 6 min, and 96 % of the BPs were adsorbed to the host cells within 12 min. Marzia et al., found a similar pattern for the adsorption rate of BP SAP-26 on the surface of *S. aureus* (WS-05 strain) bacteria. The study revealed that over 95 % of SAP-26 BP adsorbed to the susceptible strain of *S. aureus* within 9 min [69]. Imam et al., found that BP (MIJ3) exhibited a 95 % adsorption rate on the surface of *P. aeruginosa* host cells within 20 min [70].

3.2.5. Singular step growth curve

To assess the growth rate of BPSAΦ1 and BPPAΦ1, as well as the latent period and burst size per infected bacterial cell, the singular-step growth curves of the study were performed. The obtained data were analyzed, and triphasic curves were plotted (Fig. 1F), it was observed that the BPSAΦ1 and BPPAΦ1 had a latent period of 30 and 15 min. In terms of burst size, BPSAΦ1, and BPPAΦ1 exhibit 75 and 112 PFUs per infected host cell. The burst size and latency period are essential factors to consider in the context of BPs potential therapeutic applications. Han et al. found that *Staphylococcus* bacteriophage SAH-1 had 20 min latent period and 100 PFU/cell burst size [71]. The same factors were also observed for the BP SA (30 min, 1000 PFU/cell) and MSA6 (15 min, 23 PFU/cell) [72,73]. The higher burst size and shorter latent duration are thought to be advantageous, although there are situations when the host bacterial cell density is low and a prolonged latent period is required [74].

3.2.6. pH, temperature, and U.V. stability studies of bacteriophage

This study was carried out to determine the optimal pH and temperature for the development of BP formulations. The PFU of both BP (BPSAΦ1 and BPPAΦ1) titer was higher in the range of pH 6.8–7.4 and a temperature range of 4–40 °C, but no active BP was found at pH 1.5, pH 9.5, and above 80 °C (Fig. 1(G) and (H)).

Furthermore, within 5 min following UV exposure, the BP titer decreased to half of the initial titer and reached to non-measurable limit within 10 min indicating the poor acceptability of the UV sterilization for the BP formulations. The formulation can be prepared within pH 6.8–7.4 at a temperature below 40 °C. A similar study conducted by Feng et al., investigated the impact of temperature and pH on the viability of coliphages (MS2 and Qβ) in both wastewater and water. The BPs exhibited the lowest inactivation rate when subjected to pH levels ranging from 6 to 8 and temperature ranges between 5 °C–35 °C [75]. Furthermore, several studies have shown that pH values below 4 and above 9, as well as temperatures above 40 °C, generally restrict BP activity and viability [76–78]. The highly acidic pH and extreme temperature cause protein denaturation and destruction which compromises the BPs ability to regulate biologically [79].

3.2.7. Hemocompatibility assay of bacteriophages

The hemolysis study suggested the hemocompatibility nature of the BPs. According to national biological safety guidelines, if the rate of hemolysis is <2 %, the BPs are classified as non-hemolytic. The hemolysis rates of BPSAΦ1 and BPPAΦ1 BPs were found to be 1.06 ± 0.08 and 0.91 ± 0.014, respectively. The hemocompatibility study demonstrated that BPs are hemocompatible and nonhemolytic to RBCs (Fig. 2).

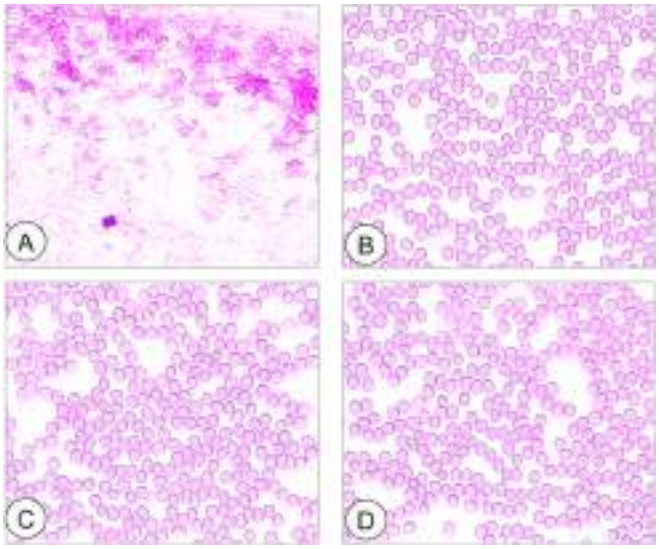

Fig. 2. Represents the images of the hemocompatibility study (40× resolution), where (A) positive control group (distilled water), (B) negative control group (normal saline), (C) BPSAΦ1 BP, and (D) BPPAΦ1 BP.

3.3. Formulation and characterization

The chitosan microparticles were developed by the ionic gelation method in the presence of STPP. BPs were dispersed in the polymeric solution of the chitosan and the gradual addition of the STPP under magnetic stirring triggered the ionic crosslinking of the chitosan amine groups (positively charged) and phosphate groups (negatively charged) of the STPP while the dispersed BPs got entrapped inside the polymeric matrix during the crosslinking and formation of chitosan microparticles.

BPs and excipients (chitosan, trehalose, STPP, glycerol, and Sepineo™ P 600) compatibility study was performed by incubating the BP in the presence of excipients for 24 h at 37 °C. It was observed that there was no significant decrease in the titer of BP. This observation strongly suggests that the selected excipients used in the formulation are compatible with BP. The absence of any decline in the titer indicates that the excipients do not negatively impact the stability or viability of the BPs. The data for particle size, PDI, zeta potential, and entrapment efficiency of the optimized formulation have been presented in Table 2. Further, the prepared MPs were incorporated into the Sepineo™ P 600 gel. Based on the effectiveness of the BPs entrapment as well as its

Table 2
Particle size, Polydispersity, Zeta potential, and entrapment efficiency of developed MPs.

Formulations	Particle size (μm) (Mean ± SD*)	Polydispersity (Mean ± SD*)	Zeta potential (mV) (Mean ± SD *)	EE% (Mean ± SD *)
Blank CHMPs	0.845 ± 0.264	0.254 ± 0.086	18.20 ± 0.249	–
BPSAΦ1-CHMPs	1.197 ± 0.117	0.454 ± 0.015	26.36 ± 0.207	88.68 ± 1.17
BPPAΦ1-CHMPs	1.423 ± 0.210	0.196 ± 0.047	29.04 ± 0.368	82.55 ± 1.22
MBP-CHMPs	2.846 ± 0.288	0.431 ± 0.066	32.11 ± 0.593	87.56 ± 1.03 (BPSAΦ1) and 79.52 ± 0.84 (BPPAΦ1)

Data has been presented as Mean ± SD, *n = 3; SD: Standard deviation.
Blank CHMPs: Blank chitosan microparticles.
BPSAΦ1-CHMPs: Bacteriophage against *S. aureus* chitosan microparticles.
BPPAΦ1-CHMPs: Bacteriophage against *P. aeruginosa* chitosan microparticles.
MBP-CHMPs: Mixed bacteriophage chitosan microparticles.

suitability for use in both moderate and severe deeper wound infections for local effect, the BP loaded microparticle size was optimized. In addition, BP microencapsulation using chitosan and other polymers has been reported in several studies against numerous infectious diseases [41,80,81].

3.3.1. BP-CHMPs-gel characteristics

The BPSAΦ1-CHMPs-gel, BPPAΦ1-CHMPs-gel, and MBP-CHMPs-gel were found odorless, homogenous, translucent, and effortless spreadability, had a viscosity of 3298.24 ± 0.047, 3370.18 ± 0.63, and 3384.6 ± 0.88 cP, respectively. Hence, the obtained data suggested that SEPINEO™ P 600 is a good candidate for the preparation of BP microparticles-based gel formulation.

3.3.2. In vitro bacteriophage release study

The release patterns of free BPSAΦ1, BPPAΦ1, BPSAΦ1-CHMPs, BPPAΦ1-CHMPs, MBPΦ1-CHMPs, and MBPΦ1-CHMPs-gel are depicted in Fig. 3A and B. The free BPs (BPSAΦ1 and BPPAΦ1) completely released within 30 min, whereas the BP release from BPSAΦ1-CHMPs and BPPAΦ1-CHMPs were 94.81 ± 3.71 % and 91.73 ± 2.53 % respectively, in 12 h. Moreover, BP release from BPSAΦ1-CHMPs gel and BPPAΦ1-CHMPs gel showed 79.556 ± 1.960, and 73.1250 ± 1.480 % respectively, in 12 h. Furthermore, BPSAΦ1 and BPPAΦ1 release from MBP-CHMPs was 94.00 ± 2.16 and 96.16 ± 1.30 % in 12 h. Besides that, the gel effect on BP release (BPSAΦ1 and BPPAΦ1) from MBP-CHMPs-gel was investigated and observed that 74.55 ± 2.06 and 70.30 ± 1.27 % of BPSAΦ1 and BPPAΦ1 were released in 12 h, respectively. Hence, the obtained data suggested that the incorporation of the MPs in the gel further sustained the BP discharge and could produce an antibacterial activity for a longer duration. BPSAΦ1 release from both MPs was considerably higher than BPPAΦ1, which could be attributed to the smaller size of BPSAΦ1 than BPPAΦ1.

As determined by BP release kinetics, the correlation coefficient values are shown in Table 3. According to the regression coefficient values, the release kinetics of free BPs (BPSAΦ1 and BPPAΦ1) follow the first-order kinetics, and microparticles and microparticle-loaded gel formulations follow the Korsmeyer-Peppas models which confirms a combination of diffusion and erosion as the mechanism of BP release from chitosan microparticle matrix and gel.

In a study conducted by Jamaledin et al., the authors developed BPs-loaded PLGA microparticles using a double emulsification approach. A sustained release phenomenon was observed in the formulations of BP-loaded microparticles, characterized by an initial rapid release followed by a gradual and prolonged release over a period [82]. Likewise,

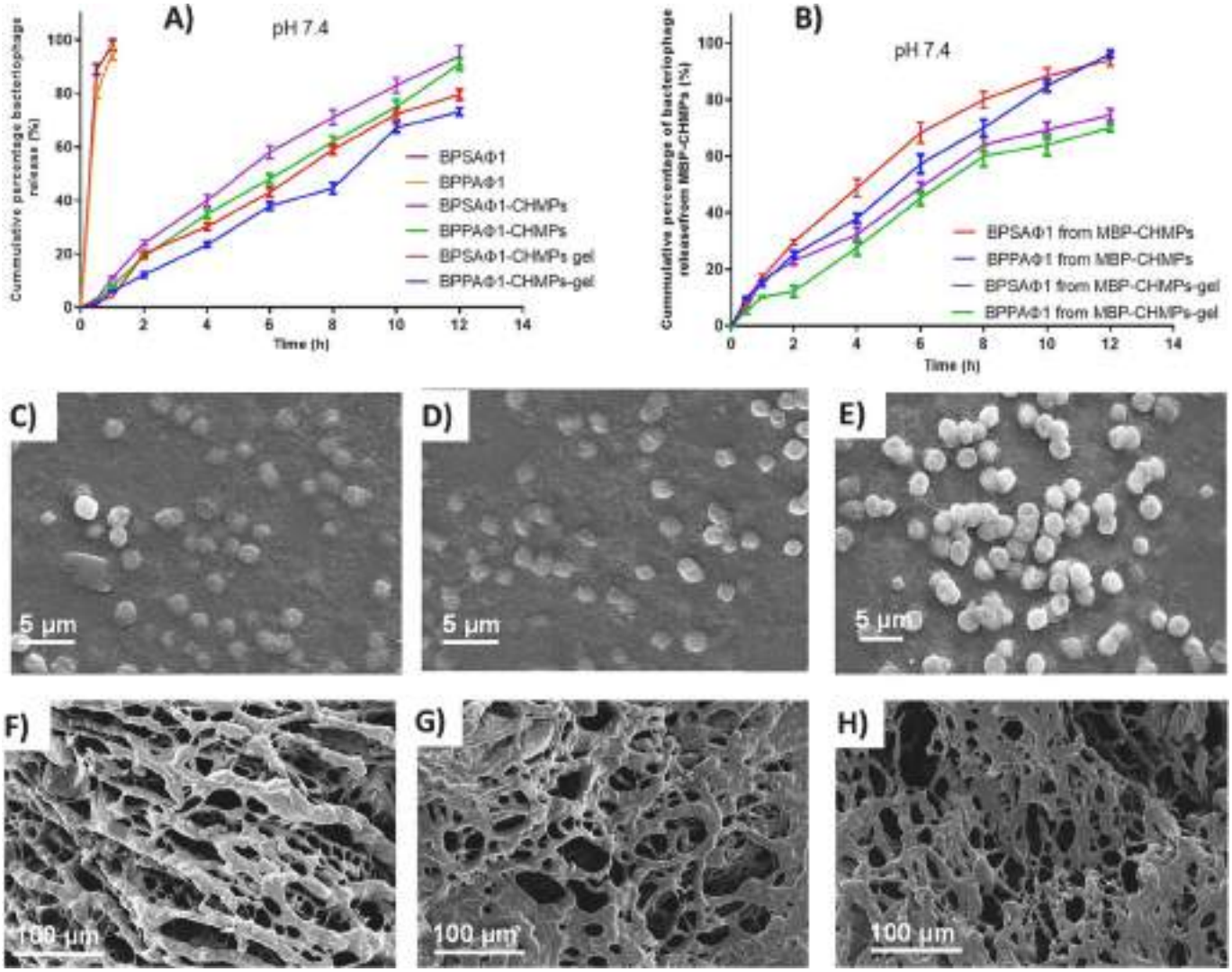

Fig. 3. *In vitro* release of the BP from A) free BP, BPSAΦ1-CHMPs, BPPAΦ1-CHMPs, BPSAΦ1-CHMPs gel & BPPAΦ1-CHMPs gel and B) BPs release profile from MBP-CHMPs and MBP-CHMPs laden gel at pH 7.4. Morphological examination of the microparticles and gel formulation. SEM images of C) BPSAΦ1-CHMPs, D) BPPAΦ1-CHMPs, E) MBP-CHMPs, F) Blank gel, and G) MBP-CHMPs loaded gel. Data for the release study has been presented as Mean ± SD (n = 3).

Table 3
Correlation coefficient values following the release data fitting in different models.

Batch	Zero-order (r^2)	First-order (r^2)	Korsmeyer-Peppas (r^2)	Higuchi (r^2)	Hixson-Crowell (r^2)
BPSAΦ1	0.7819	0.9992	0.9006	0.9159	0.8993
BPPAΦ1	0.8380	0.9984	0.8961	0.9090	0.8662
BPSAΦ1-CHMPs	0.9283	0.9109	0.9989	0.9302	0.9144
BPPAΦ1-CHMPs	0.9051	0.9033	0.9973	0.8996	0.9354
BPSAΦ1-CHMPs gel	0.8985	0.8762	0.9969	0.8944	0.8879
BPPAΦ1-CHMPs-gel	0.8902	0.8590	0.9948	0.8549	0.8973
BPSAΦ1 from MBP-CHMPs	0.9193	0.9004	0.9982	0.9277	0.9089
BPPAΦ1 from MBP-CHMPs	0.9010	0.9226	0.9961	0.9031	0.8972
BPSAΦ1 from MBP-CHMPs-gel	0.8380	0.8889	0.9958	0.9323	0.8847
BPPAΦ1 from MBP-CHMPs-gel	0.8091	0.8854	0.9930	0.9013	0.8015

Yongsheng et al., formulated BP-loaded microparticles to combat the cystic fibrosis-causing *S. aureus*. The release profile of BP, when loaded onto the microparticles, exhibited an initial burst release of the BP followed by a sustained release over 12 h [83].

3.3.3. Surface morphology

The MPs were scanned using SEM to determine their surface morphology. Formulated MPs (Fig. 3C, D, E) were observed to be homogeneous with somewhat spherical. An interwoven network of irregular fibers was observed in the blank gel and MBP-CHMPs gel (Fig. 3F and G). The spaces observed in the interwoven network of MBP-CHMPs gel were less than blank gel and might be ascribed to the incorporation of the MPs in these spaces. Martins et al. reported similar observations of irregularly shaped large clusters in chitosan/tripolyphosphate microparticles [84]. However, the type, quantity, and formulation procedure as well as the solvent environment all affect the morphology of chitosan microparticles [85].

3.4. In vitro antibacterial studies

3.4.1. Spot test

Spot tests were performed to evaluate the formulation qualitative antibacterial activity efficacy. Blank CHMPs showed unclear little (2 ± 0.08 mm) while the blank gel had no antimicrobial action, whereas BPSAΦ1-CHMPs (10.46 ± 1.36 mm) and BPPAΦ1-CHMPs (12.12 ± 1.02 mm) both exhibited antibacterial activity against *S. aureus* and *P. aeruginosa*, respectively. Moreover, MBP-CHMPs (12.63 ± 0.75) and MBP-CHMPs-gel (13.33 ± 0.56) showed antibacterial efficacy against both bacteria. In addition, several studies have shown the efficacy of spot tests for determining the lytic activity of BPs against specific bacterial strains [68,86–91].

3.4.2. MIC and MBC

The MIC values of BPSAΦ1-CHMPs, BPPAΦ1-CHMPs, and MP-CHMPs, following 24 h of incubation, were found to be 150 ± 2.03, 170 ± 1.08, and 160 ± 1.81 μg/μL, respectively (Table 4). Further, obtained MBC values of BPSAΦ1-CHMPs, BPPAΦ1-CHMPs, and MP-CHMPs were 180 ± 2.01, 185 ± 1.09, and 175 ± 1.05 μg/μL, respectively. The findings revealed no synergistic or antagonistic interaction between BPs (BPSAΦ1 and BPPAΦ1).

Table 4
Antibacterial activity of the developed BP loaded MPs.

Formulation	MIC (μg/μL)	MBC (μg/μL)	Biofilm eradication (%)
Blank CHMPs	–	–	10.01 ± 0.3
BPSAΦ1-CHMPs	150 ± 2.03	180 ± 2.01	88.43 ± 1.04
BPPAΦ1-CHMPs	170 ± 1.08	185 ± 1.09	81.31 ± 0.53
MBP-CHMPs	160 ± 1.81	175 ± 1.05	85.68 ± 0.28

MBP-CHMPs showed MIC as 160 ± 1.81 μg/μL against a mixture of *S. aureus* and *P.* indicating that BPSAΦ1-CHMPs and BPPAΦ1-CHMPs formulations are independently active against respective bacteria. MBP-CHMPs showed intermediate activity, which is higher than BPSAΦ1-CHMPs and lower than BPPAΦ1-CHMPs. The study conducted by Luo et al. assessed the MIC of BP YC#06, antibiotic, and their combination against *A. baumannii* bacteria. It has been found that the MIC of antibiotics decreased when combined with BP due to the synergistic effect [92]. Although, treating polybacterial infections is more difficult and challenging than treating infections caused by a single bacterial infection [93].

3.4.3. Antibiofilm assay

The formation of biofilms over burn wound sites is one of the main causes of burn treatment failures. The success of the treatments is governed by the eradication of the biofilm from the wound. This study was carried out to evaluate the antibiofilm potential of the developed formulation against the biofilm that was grown for 48 h (Fig. 4A).

The results depicted that BPSAΦ1-CHMPs, BPPAΦ1-CHMPs, and MBP-CHMPs had significant ($P < 0.05$) biofilm eradication with 88.43 ± 1.04, 81.31 ± 0.53, and 85.68 ± 0.28 %, respectively. In contrast, after 24 h of treatment, the blank CHMP-treated group showed only 10.01 ± 0.3 % eradication of *S. aureus* biofilm, 7.41 ± 0.38 % eradication of *P. aeruginosa* biofilm, and 6.62 ± 0.94 % eradication of mixed biofilm, which is insignificant as compared with the control biofilm. (Table 4, Fig. 4A). Further study also revealed that the developed formulation prevents biofilm formation by >90 %. BPs prohibit biofilm development by a) inhibiting cell-to-cell signaling (quorum sensing), b) penetrating mature biofilms, c) producing EPS degrading enzymes, endolysins, hydrolase, and polysaccharide depolymerase, d) lysing the bacterial cell, and e) host specific lytic activity [94–96]. Chitosan has an anti-biofilm effect because of the functional amino groups of *N*-acetyl-glucosamine units. The positive charge of chitosan reacts electrostatically with the negatively charged biofilm components such as EPS, DNA, and proteins, resulting in bacterial biofilm inhibitory action [97]. Several studies suggest that using BP in combination with chitosan could improve their effectiveness. Abdelsattar et al. conducted a similar investigation and discovered that chitosan and BP have additive inhibitory effects on Gram-positive and Gram-negative bacteria and the formation of biofilms [98]. According to Adnan et al. findings, treatment with MA-1 BP for 6 h resulted in a significant eradication (99.9 %) of 74-h-old biofilms when compared to the control group [99].

3.4.4. Microscopy of biofilm

Morphological evaluation of biofilms provides valuable insights into the spatial arrangement that occurs within them as well as with the supporting surfaces. Biofilm grown on a glass slide was observed by the SEM, CLSM, and AFM (Fig. 4). CLSM (Live/dead staining) images show thick live bacteria green structures in control groups (untreated) of *S. aureus* (Fig. 4C, first row), *P. aeruginosa* (Fig. 4C, second row), and combination of these two bacteria (Fig. 4C, third row). Treatment with BPSAΦ1-CHMPs, BPPAΦ1-CHMPs, and MBP-CHMPs depicted dead bacteria in red color with reduced biofilm thickness.

Additionally, SEM (Fig. 4B) and AFM (Fig. 4D) analysis found that control biofilms (*S. aureus* cells (spherical), *P. aeruginosa* (rod), and a mix of both bacteria (spherical and rod demonstrated intricate arrangements of multi-layered cell clusters intertwined within a matrix composed of

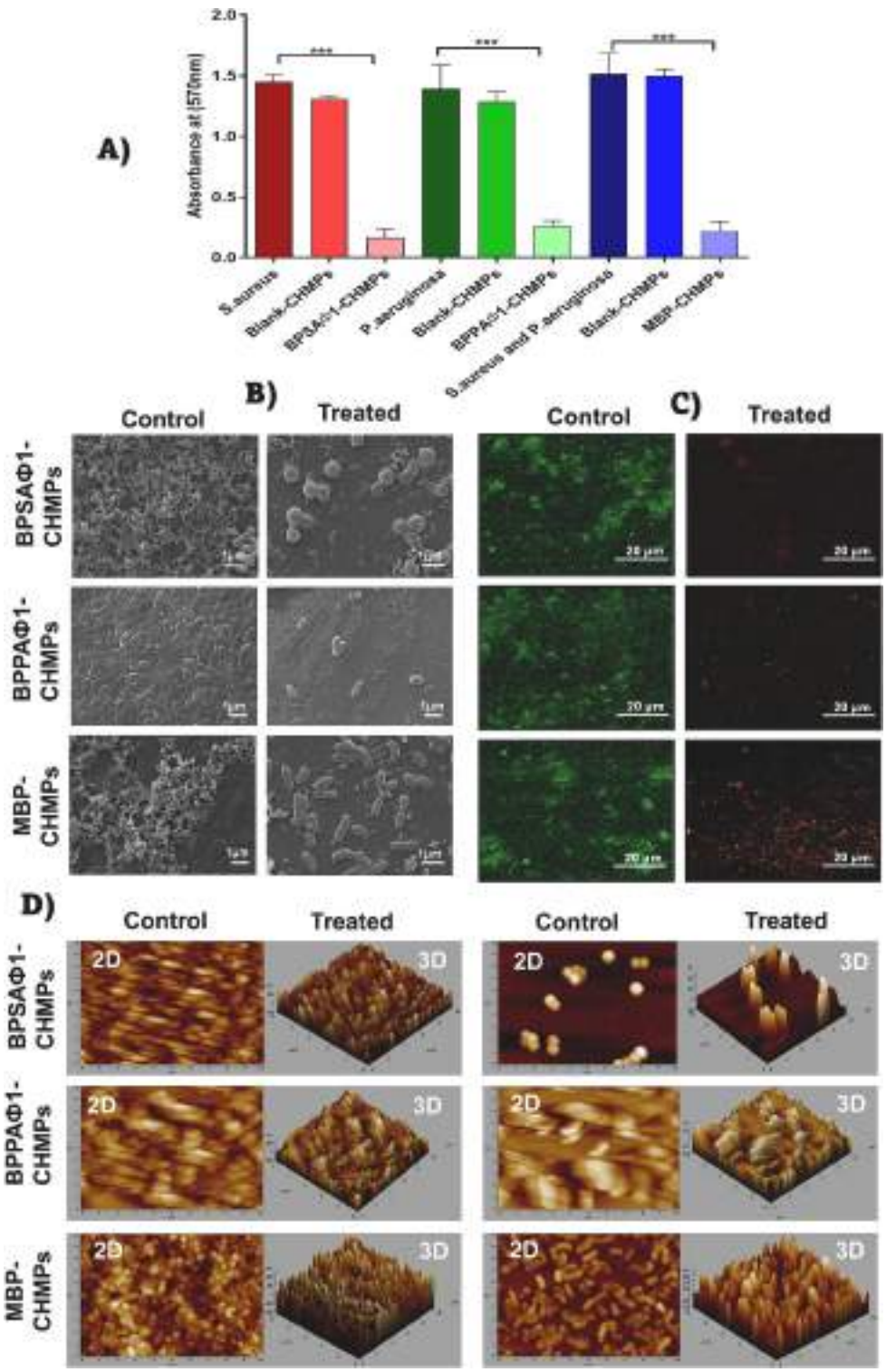

Fig. 4. Antibiofilm effect of BPs formulations BPSAΦ1-CHMPs, BPPAΦ1-CHMPs, and MBP-CHMPs on *S. aureus*, *P. aeruginosa* and a mixed bacterium (both), respectively, were observed by different microscopy techniques, where (A) treatment effect of different BPs formulations on biofilms, (B) scanning electron microscopy of untreated and treated biofilms (C) represents confocal laser scanning microscopy (SYTO 9 green is indicative of live cells while P.I. red is indicative of dead bacteria) and (D) Atomic force microscopy of control and treated biofilms with 2D & 3D representation (20 × 20 μm area). The control group did not receive any treatment, and the treatment group was treated with BPs microparticle formulations. Data is shown as mean ± SD (n = 3). The statistical analyses were conducted using a one-way analysis of variance (ANOVA). *** indicates the $p < 0.001$ as compared to the negative control. (For interpretation of the references to color in this figure legend, the reader is referred to the web version of this article.)

extracellular biological substances before treatment. Following incubation with the different BP formulations, biofilm was significantly reduced compared with the control group. It was also observed that mixed bacterial biofilm was more dense than individual bacterial biofilm. The result suggested that MBP-CHMPs were effective against the mixed polybacterial biofilm. Biofilms typically demonstrate a greater proportion of persisters cells compared to planktonic populations, thereby enhancing their capacity to endure antimicrobial challenges [100]. In a recent study conducted by Duarte et al., the researchers investigated the combined impact of BP phiIPLA-RODI and the BP-derived lytic protein CHAPSH3b on robust biofilm formation by *S. aureus*15981 and *S. aureus* V329 strains [101]. The researchers conducted a visual examination of the 24-h-old biofilms using confocal laser scanning microscopy (CLSM). They observed that the combination treatment resulted in the greatest degree of bacterial cell death. Furthermore, a plethora of research studies have been conducted to demonstrate the advantages of utilizing SEM, CLSM, and AFM for the visual examination and eradication of their intricate structures [100,102–105].

3.4.5. Cytotoxicity study

The toxicity of the isolated BPs and formulations was assessed on mammalian cell lines with the use of HEK-293 cells. The cells were exposed to BPSAΦ1 and BPPAΦ1, as well as BPSAΦ1-CHMPs, BPPAΦ1-CHMPs, and MBP-CHMPs formulations (Fig. 5). Additionally, a positive control of 1 % Triton X-100 and a negative control of PBS were used. The results obtained from the MTT assay indicated that there were no major differences in the morphology of the cells treated with the BP, all formulations, and PBS (Fig. 5A) after a 24-h incubation period. However, a positive control (1 % triton X-100) showed just 2.5 % cell viability (Fig. 5B). The results of the analysis indicate that both the BP and their formulations do not exhibit cytotoxic effects (>90 % viability, Fig. 5B). Furthermore, prior studies have also reported the absence of any cytotoxic impact of BPs such as vB_SauM-A, vB_SauM-C, vB_SauM-D on Bj cells [106], BP phiCDHS1 on HT-29 cells [107], and BPs PφEn-CL and PφEn-HO on A375 and HFSF-PI 3 cells [108].

3.5. Stability studies

The stability study (Fig. 5C) results indicated that the pure BP suspension were found unstable due to the decrease in >50 % of BPs titer

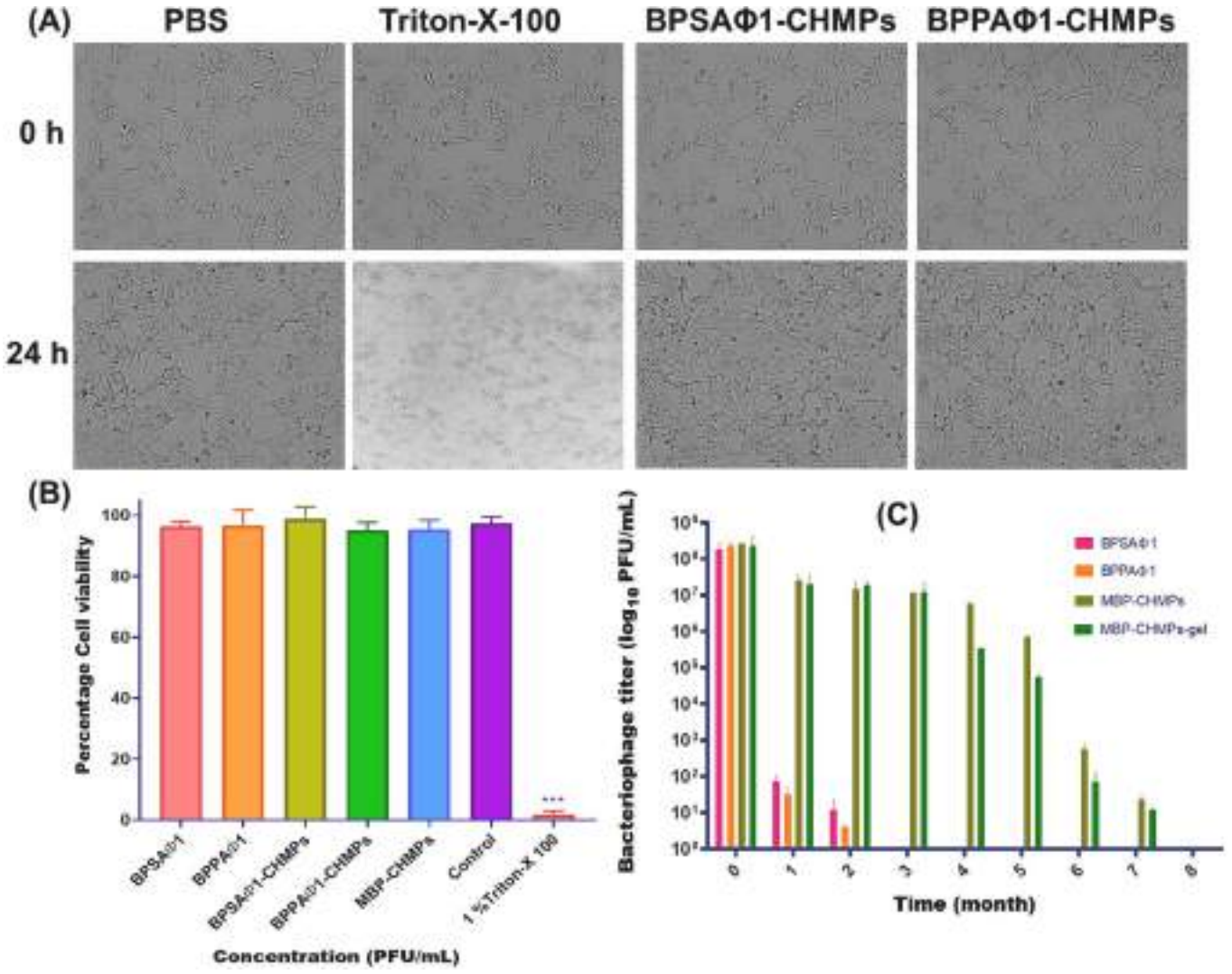

Fig. 5. Cytotoxicity of isolated bacteriophage and developed formulations on mammalian cells was studied with Human Embryonic Kidney (HEK293) cells (10^5 cells/well) using MTT assay, where (A) Cell images show that there is no change in their morphology after bacteriophage treatment as compared to the controls, (B) Comparing mammalian cell survival concerning different treatments C) Stability studies of pure BP solution, MBP-CHMPs, and MBP-CHMPs-gel. Data is shown as mean ± SD (n = 3). The statistical analyses were conducted using a one-way analysis of variance (ANOVA). *** indicates the $p < 0.001$ as compared to the negative control.

within a month at 4.0 ± 0.2 °C, while a complete loss of activity was observed in 3 months. In the case of MBP-CHMPs and MBP-CHMPs-gels, the titer decreased by one-tenth in the first month. However, it was maintained for up to 4 months when stored at 4.0 ± 0.2 °C, and this stability could be attributed to the protective nature of trehalose and glycerine present in the developed formulation. Several reports have suggested that the addition of trehalose enhances the stability of BPs [109–111]. The results demonstrated that trehalose exhibited a decrease in the accumulation of reactive oxygen species and protein oxidation products throughout storage. Trehalose-based BP antimicrobial films/coatings exhibit significant promise in the extended preservation of BPs [112].

3.6. In vivo study

The evaluation of burn wound healing is a crucial aspect of assessing the progress and effectiveness of burn wound treatment. It involves a comprehensive assessment of two primary factors: the area of the burn and the depth of the burn. The percentage of wound closure (Fig. 6) after treatment with BPSAΦ1-CHMPs-gel (Group-III), BPPAΦ1-CHMPs-gel (Group-IV), and MBP-CHMPs-gel (Group-V) were found to be 84.61 ± 1.03 %, 83.38 ± 1.87 %, and 85.54 ± 0.05 % on 28th day, whereas

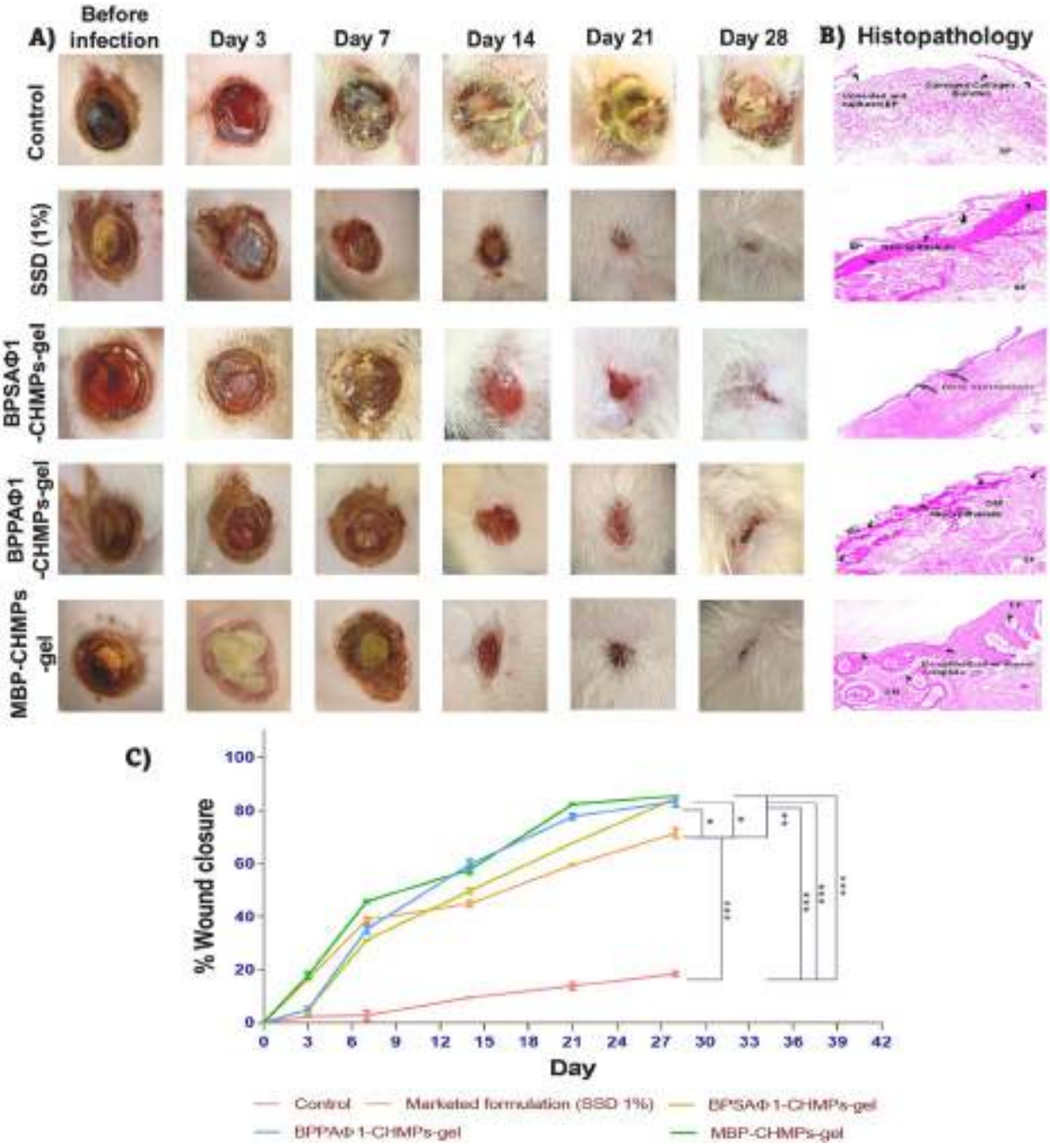

Fig. 6. Burn wound healing assay. A) Effect of BP formulations in burn wound on different days, B) histopathology examination at the end of the healing where arrow mark shows damaged collagen bundles with ruptured epithelium in the control group and formation of new epithelium membrane in other groups. C) The graph depicts the percentage of wound closure with time (days). Data is shown as mean ± SD (n = 3). The statistical analyses were conducted using a one-way analysis of variance (ANOVA). $p < 0.001$ (***), $p < 0.01$ (**), and $p < 0.05$ (*) as compared to the control untreated group.

marketed formulation (Group-II) treated animals had 71.47 ± 1.75 % of wound closure. The control group also showed around 18 % wound contraction however, pus formation was also noticed with time. Moreover, the results confirmed the effectiveness of BPs combination in the treatment of polybacterial infections.

Furthermore, microscopic images of H & E stained rat skin (Fig. 6B) depicted quicker and complete re-epithelialization of the BPSAΦ1-CHMPs-gel, BPPAΦ1-CHMPs-gel, MBP-CHMPs-gel treatment group in comparison with the commercially available product. In contrast, untreated rats (Fig. 6B) did not exhibit full re-epithelialization by day 28. In a previous report, lytic phases φAB140 and φAB150 chitosan formulation showed a significant decrease in wound size having MDR bacterial infection [41]. In a recent study conducted by Rezk et al., it was discovered that BP ZCPA1 exhibits an effective antibacterial agent against multidrug-resistant *P. aeruginosa*. The study further demonstrated that the application of BP ZCPA1 resulted in significant improvements (99.84 %) in wound healing effects in a rat model with full-thickness infection of a wound [113]. Antibiotic ineffectiveness in antimicrobial-resistant wound infections imposes an immense medical and financial burden, highlighting the need for new treatments to remove obstacles to wound healing in wound care.

A 3D-Mode of Ultrasound (USG) was used for collecting two-dimensional (area) and three-dimensional (depth and volume) data on the wound. PA-Mode was for determining saturated oxygen percentage (sO_2%). USG imaging was used for locating the wound and measuring its volume(mm^3) on the 3rd, 14th, and 21st days. The obtained data were processed by using Vivo Lab software (Fig. 7), and the wound volume data were plotted against the day. On day 3, the wound volumes of control (Group-I), 1 % SSD (Group-II), BPSAΦ1-CHMPs-gel (Group-III), BPPAΦ1-CHMPs-gel (Group-IV), and MBP-CHMPs-gel (Group-V) was found to be 481.40 ± 12.12, 444.68 ± 16.0, 469.276 ± 27.9, 442.25 ± 25.14, and 425.23 ± 23.12 mm^3, respectively. The volumes of the wound after treatment with BPSAΦ1-CHMPs-gel (20.161 ± 1.24 mm^3), BPPAΦ1-CHMPs-gel (34.60 ± 0.92 mm^3), and MBP-CHMPs-gel (14.16 ± 1.40 mm^3) were reduced significantly in day 21. The scar of the healed wound was visible in the 2D and 3D USG images (Fig. 7C, D, and E). Moreover, after treatment with 1 % SSD, wound volume was found to be 87.02 ± 9.54 mm^3, which was higher than BPs and their MPs, and the untreated group shows an increase in wound volume (494.74 ± 12.20 mm^3) (Fig. 7F) due to heavy infection.

The USG images provided clear visual evidence of significant damage to the deeper layers of the skin on day 3. As the burn wound underwent the recovery process, a gradual reduction in burn depth was observed, reaching its noticeable decline by day 14. After 21 days, burn depth has been gradually reduced after treatment with BP formulation. Therefore, BP formulations have demonstrated efficacy in treating antibiotic-resistant bacterial wound infections caused by specific strains.

PA imaging (Fig. 8) is an excellent technique for effectively observing and assessing the progress of localized blood vessel formation, blood flow, and the level of oxygen saturation. These specific parameters play a crucial role in the healing process of wounds. The day 3 oxygen saturation (sO_2%) of control, 1 % SSD, BPSAΦ1-CHMPs-gel, BPPAΦ1-CHMPs-gel, and MBP-CHMPs-gel groups (Fig. 8) were found to be 24.41 ± 1.08, 30.403 ± 1.3, 29.824 ± 2.33, 19.63 ± 2.13, and 21.1 ± 1.82 %, respectively. sO_2% gradually increased as the day of treatment progressed, and the level of sO_2% was higher in formulation-treated groups, BPSAΦ1-CHMPs-gel (81.20 ± 0.74 %), BPPAΦ1-CHMPs-gel (75.40 ± 0.94 %), MBP-CHMPs-gel (89.45 ± 0.40 %) as compared to marketed

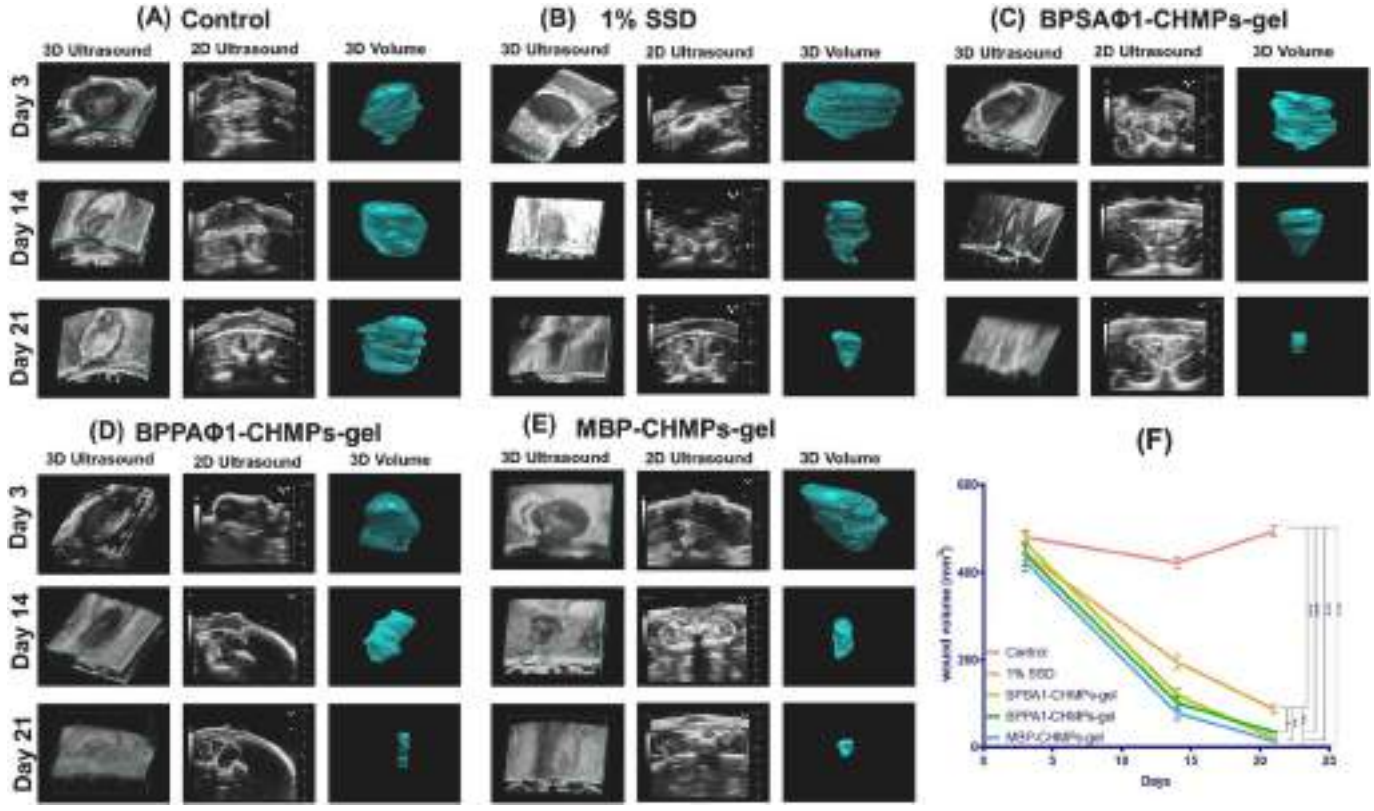

Fig. 7. Ultrasound imaging of infected burn wound where (A) represents the control group (without treatment), (B) treated with 1 % SSD (marketed formulation), (C) treated with BPSAΦ1-CHMPs-gel, (D) treated with BPPAΦ1-CHMPs-gel and (E) treated with MBP-CHMPs-gel. Each group represents a 3D ultrasound image, a 2D ultrasound image captured by using the 3D ultrasound mode, and the wound volume measured by the multislice method on 3, 14, and 21 days. (F) graphical representation of quantitative measurement of wound volume on different days. The standard deviation is shown in the error bars (n = 5). Data is shown as mean ± SD (n = 3). The statistical analyses were conducted using a one-way analysis of variance (ANOVA). $p < 0.001$ (***), $p < 0.01$ (**), and $p < 0.05$ (*) as compared to the control untreated group.

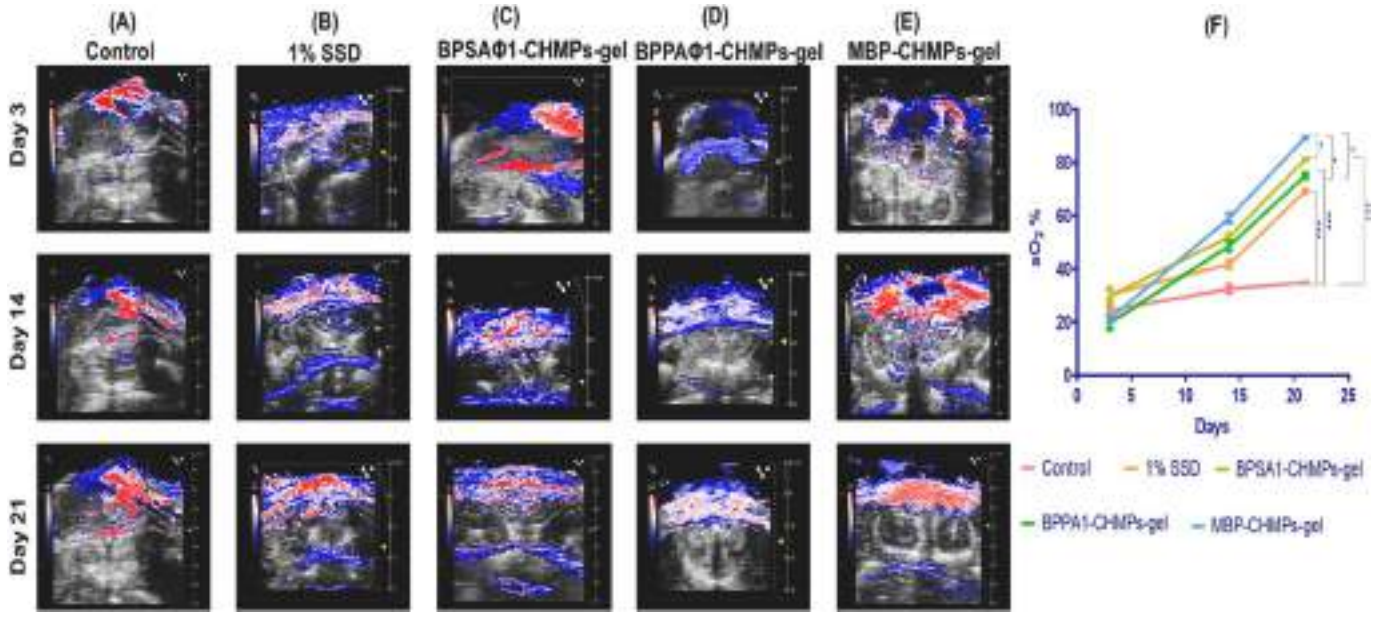

Fig. 8. Ultrasound and Photoacoustic imaging of infected wound where, (A) Control group (without treatment), (B) treated with 1 % SSD (marketed formulation), (C) treated with BPSAΦ1-CHMPs-gel (D) BPPAΦ1-CHMPs-gel and (E) treated with MBP-CHMPs-gel. (F) graphical representation of quantitative oxygen saturation measurement on days 3, 14, and 21. Data is shown as mean ± SD (n = 3). The statistical analyses were conducted using a one-way analysis of variance (ANOVA). $p < 0.001$ (***), $p < 0.01$ (**), and $p < 0.05$ (*) as compared to the control untreated group.

formulation (69.25 ± 0.54 %) and control group (34.89 ± 0.81 %) on day 21. More interestingly, during the initial week, the central region of the burn exhibited higher levels of hypoxia when compared to the surrounding area. This was mainly caused by dermal damage and a lack of blood perfusion. The sO_2% increased with increasing post-burn days due to the recovery of blood perfusion. Existing literature highlights the relevance of USG/PA imaging as an emerging tool for analyzing wound healing. A multiscale photoacoustic assessment was used to determine the efficacy of the chitosan-graphene oxide (CH-Go) hemostatic sponge. After analyzing the data, they concluded that the Chi-GO hemostatic sponge showed promising results in terms of hemostatic application, wound therapy, and targeted medication release [114]. Mantri et al. evaluated the use of PA-US to track angiogenesis in 19 clinical patients. In this study, local angiogenesis, tissue perfusion, and oxygen saturation were studied for 3 weeks along with a 3D map of wound bed physiology. They concluded that PA imaging is the most effective method for predicting wound healing. This imaging may help clinicians decide whether to start, continue, adjust, or stop therapy earlier [115]. Usually, clinicians assess wound health based on surface indications such as color, odor, skin texture, discharge, edema, and the presence of weakened tissue.

3.7. Gel occlusion and bio-imaging study

In this study, DiD dye (fluorescent dye) was used as a model dye for fluorescent imaging. DiD dye-loaded MPs and microparticles-laden gels were evaluated for sustained fluorescent signal and correlating with BP release or sustained activity on the wound of rat (Fig. 9). From fluorescent imaging (Fig. 9A), it was observed that DiD-CHMPs and DiD-CHMPs-gel (gel) both are site-specific and not distributed to other body organs when evaluated up to 6 h. Moreover, DiD-CHMPs-gel was not only easy to apply but also remained on the wound site (fluorescent intensity 3.69e7 ± 100,250–1.27e6 ± 45,900) for >6 h without any significant loss of fluorescent intensity. However, DiD-CHMPs formulation after its application shows a gradual decrease in the fluorescent intensity with time, more significantly compared to the microparticle loaded gel (Fig. 9B). On the contrary, DiD-CHMPs was a little inconvenient to apply, retain only in a corner portion of wound and came off in 4 h with faster decrease in fluorescent intensity from 2.65e7 ± 98,600 to 3.2e2 ± 80. Hence, from the obtained results, the conclusion can be drawn that the gel formulation exhibited a longer retention time of 6 h compared to the commonly used free DiD. This extended retention can be attributed to the formation of a gel layer around the skin when the gel is applied. Puthia et al. used *in vivo* bioimaging to evaluate the efficiency of a TCP-25 peptide-functionalized hydrogel in treating *S. aureus* and *P. aeruginosa*-infected partial-thickness wounds. They examined the TCP-25 biodistribution *in vivo* after injecting SKH1 mice dorsum with TCP-25 gel that has been Cy5-labeled. The diffusion of the peptide from the gel into the surrounding tissues was tracked using longitudinal IVIS bioimaging. The findings indicated that TCP-25 exhibited significant retention at the site of administration [116].

BPs therapy has been demonstrated to be effective both as a standalone treatment and as an adjuvant therapy when used in combination with antibiotics. However, the clinical implementation of BP therapy in Western countries continues to encounter significant challenges, primarily regulatory concerns surrounding inadequate quality and safety guidelines. Additionally, obstacles arise from the instability of BP during formulation, the laborious process of quantifying BP, variations in efficacy against biofilm, the assessment of resistance, and the presence of inadequate regulatory frameworks [117]. In addition, the identification of BP genomes is crucial for the determination of resistance genes and the assessment of lytic activity against bacteria, which can increase the cost of treatment in personalized therapy.

4. Conclusion

Antimicrobial resistance in burn wound infections is a growing challenge and a leading cause of severe infections. The production of biofilms can worsen wound conditions, especially in cases of polybacterial infections. Personalized therapy may become necessary in cases where conventional antimicrobials prove ineffective. BP therapy has evolved as an effective personalized therapy in such cases; however, maintaining the biological activity throughout treatment for wound infections remains a challenge. In the present work, we successfully demonstrated the loading of more than one BP (acting on a different host) into the CHMPs without compromising their biological activity

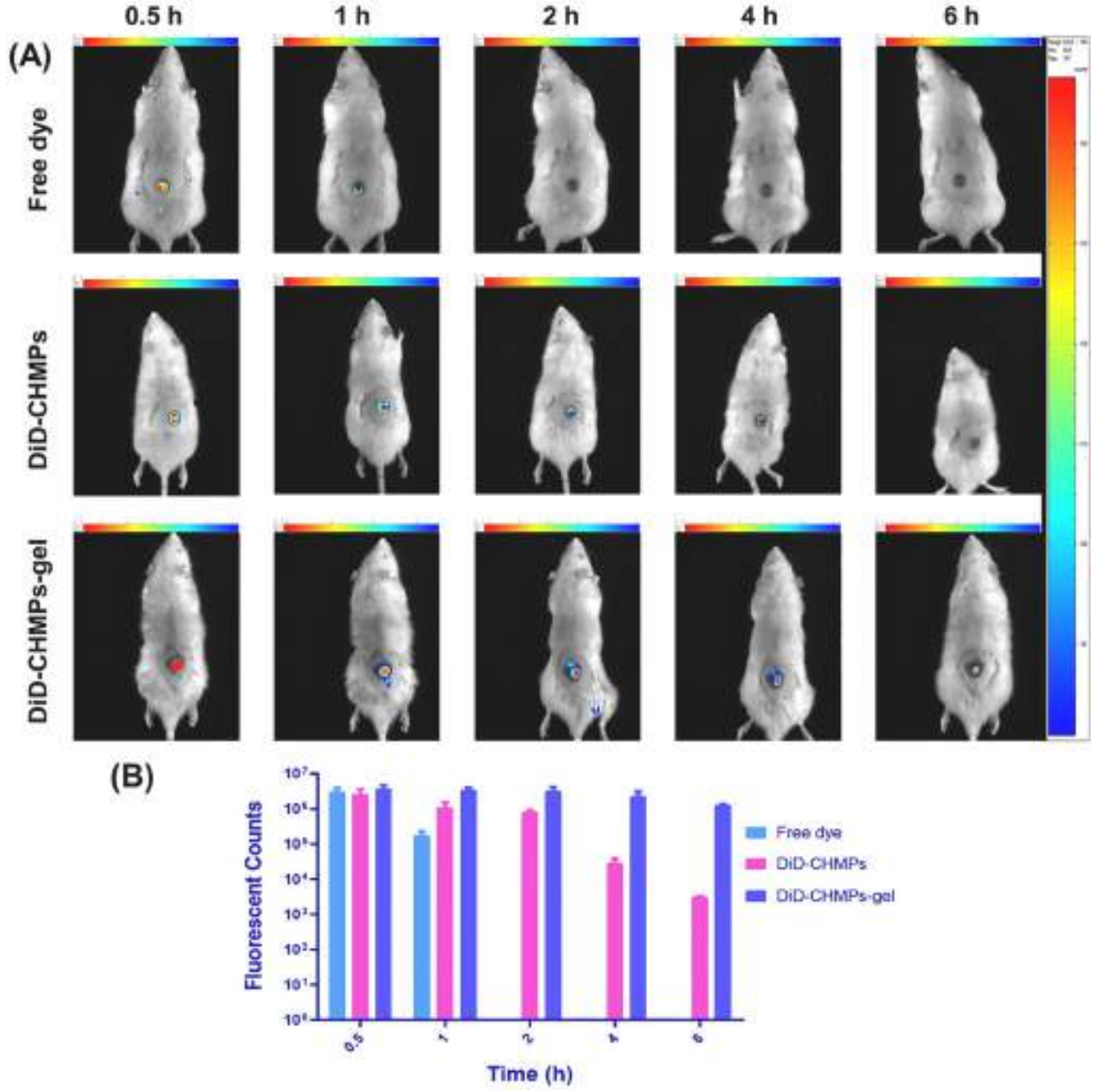

Fig. 9. (A) Fluorescent *in vivo* fluorescence imaging and gel occlusion study for 6 h following the application of the free DiD, DiD-CHMPs, and DiD-CHMPs-gel on the wounds. (B) Graphical representation of fluorescence intensity of free DiD, DiD-CHMPs, and DiD-CHMPs-gel after application to the wound at different time intervals.

and efficacy in polybacterial infections. The stability study also showed that the prepared formulations maintained their biological activity for up to four months. A series of studies demonstrated the superior efficacy of the developed formulation as compared to the marketed formulation; SSD (1 %) is considered a gold standard for treating burn wound infections. The proposed formulation strategy may not be applicable in general but can certainly be employed for personalized therapy when conventional treatment options prove ineffective. Additionally, the time-consuming process of identifying phages for each bacterial strain limits the study; however, this limitation can be addressed through the establishment of a phage bank.

Ethical declaration

All animal testing was authorized by the IAEC of IIT BHU, Varanasi-221,005, with clearance number IIT(BHU)/IAEC/2022/007.

CRediT authorship contribution statement

Deepa Dehari: conceptualization, methadology, formal analysis and data curation, and writing, Aiswarya Chaudhuri and Dulla Naveen Kumar: formulation, data collection, participated in animal experiments, Akshay Kumar & Rajesh Kumar: bacterial strain collection, phage isolation and data curation, Dinesh Kumar: validation, review & editing, Sanjay Singh: review & editing, Gopal Nath: Provided microbiology lab

facility, conceptualization, supervised, writing – review & editing and Ashish Kumar Agrawal: conceived and supervised the project, reviewing, editing, and approved the final manuscript. All authors have given approval to the final version of the manuscript.

Declaration of competing interest

The authors declare that they have no known competing financial interests or personal relationships that could have appeared to influence the work reported in this paper.

Acknowledgement

The authors acknowledge, MHRD, Govt of India, and IIT BHU, Varanasi, for providing teaching assistantship to Deepa Dehari. We also acknowledge CIF-IIT BHU for assisting in the instrumental characterization of the formulations. Additionally, we acknowledge the Department of Microbiology, IMS BHU for providing facilities to carry out the BP-related research work. We are very grateful to Professor Subash Chandra Gupta of the Department of Biochemistry at the Institute of Science, Banaras Hindu University for providing HEK-293 cell lines. We are thankful to the SATHI-BHU for providing ultrasound and photoacoustic *in vivo* imaging systems.

Appendix A. Supplementary data

Supplementary data to this article can be found online at https://doi.org/10.1016/j.ijbiomac.2023.127247.

References

[1] D.G. Greenhalgh, Management of burns, N. Engl. J. Med. 380 (24) (2019) 2349–2359, https://doi.org/10.1056/NEJMra1807442.
[2] A. Markiewicz-Gospodarek, M. Kozioł, M. Tobiasz, J. Baj, E. Radzikowska-Büchner, A. Przekora, Burn wound healing: clinical complications, medical care, treatment, and dressing types: the current state of knowledge for clinical practice, Int. J. Environ. Res. 19 (3) (2022) 1338, https://doi.org/10.3390/ijerph19031338.
[3] S. DeLeon, A. Clinton, H. Fowler, J. Everett, A.R. Horswill, K.P. Rumbaugh, Synergistic interactions of *Pseudomonas aeruginosa* and *Staphylococcus aureus* in an in vitro wound model, Infect. Immun. 82 (11) (2014) 4718–4728, https://doi.org/10.1128/iai.02198-14.
[4] P.M. Alves, E. Al-Badi, C. Withycombe, P.M. Jones, K.J. Purdy, S.E. Maddocks, Interaction between *Staphylococcus aureus* and *Pseudomonas aeruginosa* is beneficial for colonisation and pathogenicity in a mixed biofilm, Pathog. Dis. 76 (1) (2018), https://doi.org/10.1093/femspd/fty003.
[5] B. Lashtoo Aghaee, M.Y. Alikhani, W.B. van Leeuwen, A. Mojtahedi, S. Kazemi, M.M. Karami, Conventional treatment of burn wound infections versus phage therapy, Iran. J. Med. Microbiol. 16 (3) (2022) 186–196.
[6] T. Ferry, C. Kolenda, F. Laurent, G. Leboucher, M. Merabischvilli, S. Djebara, C.-A. Gustave, T. Perpoint, C. Barrey, J.-P. Pirnay, Personalized bacteriophage therapy to treat pandrug-resistant spinal Pseudomonas aeruginosa infection, J. Nat. Commun. 13 (1) (2022) 1–6.
[7] I. Aranaz, A.R. Alcántara, M.C. Civera, C. Arias, B. Elorza, A. Heras Caballero, N. Acosta, Chitosan: an overview of its properties and applications, Polymers (Basel) 13 (19) (2021) 3256, https://doi.org/10.3390/polym13193256.
[8] D. Yan, Y. Li, Y. Liu, N. Li, X. Zhang, C. Yan, Antimicrobial properties of chitosan and chitosan derivatives in the treatment of enteric infections, Molecules (Basel, Switzerland) 26 (23) (2021) 7136, https://doi.org/10.3390/molecules26237136.
[9] H. Liu, C. Wang, C. Li, Y. Qin, Z. Wang, F. Yang, Z. Li, J. Wang, A functional chitosan-based hydrogel as a wound dressing and drug delivery system in the treatment of wound healing, RSC Adv. 8 (14) (2018) 7533–7549, https://doi.org/10.1039/c7ra13510f.
[10] Q. Meng, Y. Sun, H. Cong, H. Hu, F.-J. Xu, An overview of chitosan and its application in infectious diseases, Drug Deliv. Transl. Res. 11 (4) (2021) 1340–1351, https://doi.org/10.1007/s13346-021-00913-w.
[11] G. Rahimzadeh, M. Saeedi, M. Moosazadeh, S.M.H. Hashemi, A. Babaei, M. S. Rezai, K. Kamel, K. Asare-Addo, A. Nokhodchi, Encapsulation of bacteriophage cocktail into chitosan for the treatment of bacterial diarrhea, Sci. Rep. 11 (1) (2021) 15603, https://doi.org/10.1038/s41598-021-95132-1.
[12] S.G. Rotman, V. Post, A.L. Foster, R. Lavigne, J. Wagemans, A. Trampuz, M. G. Moreno, W.J. Metsemakers, D.W. Grijpma, R.G. Richards, D. Eglin, T. F. Moriarty, Alginate chitosan microbeads and thermos-responsive hyaluronic acid hydrogel for phage delivery, J. Drug Deliv. Sci. Technol. 79 (2023) 103991, https://doi.org/10.1016/j.jddst.2022.103991.
[13] Y. Ma, J.C. Pacan, Q. Wang, Y. Xu, X. Huang, A. Korenevsky, P.M. Sabour, Microencapsulation of bacteriophage felix O1 into chitosan-alginate microspheres for oral delivery, Appl. Environ. Microbiol. 74 (15) (2008) 4799–4805, https://doi.org/10.1128/AEM.00246-08.
[14] A.S. Abdelsattar, F. Abdelrahman, A. Dawoud, I.F. Connerton, A. El-Shibiny, Encapsulation of *E. coli* phage ZCEC5 in chitosan–alginate beads as a delivery system in phage therapy, AMB Express 9 (1) (2019) 87, https://doi.org/10.1186/s13568-019-0810-9.
[15] A.K. Mehata, S. Bharti, P. Singh, M.K. Viswanadh, L. Kumari, P. Agrawal, S. Singh, B. Koch, M.S. Muthu, Trastuzumab decorated TPGS-g-chitosan nanoparticles for targeted breast cancer therapy, Colloids Surf. B Biointerfaces 173 (2019) 366–377, https://doi.org/10.1016/j.colsurfb.2018.10.007.
[16] A.C. Daly, L. Riley, T. Segura, J.A. Burdick, Hydrogel microparticles for biomedical applications, Nat. Rev. Mater. 5 (1) (2020) 20–43, https://doi.org/10.1038/s41578-019-0148-6.
[17] S.C. Hong, S.Y. Yoo, H. Kim, J. Lee, Chitosan-based multifunctional platforms for local delivery of therapeutics, Mar. drugs 15 (3) (2017), https://doi.org/10.3390/md15030060.
[18] D. Vandenheuvel, J. Meeus, R. Lavigne, G. Van den Mooter, Instability of bacteriophages in spray-dried trehalose powders is caused by crystallization of the matrix, Int. J. Pharm. 472 (1) (2014) 202–205, https://doi.org/10.1016/j.ijpharm.2014.06.026.
[19] M.S.M. Nassar, W.A. Hazzah, W.M.K. Bakr, Evaluation of antibiotic susceptibility test results: how guilty a laboratory could be? J. Egypt. Public Health Assoc. 94 (1) (2019) 4, https://doi.org/10.1186/s42506-018-0006-1.
[20] J. Hudzicki, Kirby-Bauer Disk Diffusion Susceptibility Test Protocol 15, American Society for Microbiology, 2009, pp. 55–63.
[21] Q. Mapipa, T. Digban, N. Nnolim, U. Nwodo, Antibiogram profile and virulence signatures of Pseudomonas aeruginosa isolates recovered from selected agrestic hospital effluents, J. Sci. Rep. 11 (1) (2021) 1–11, https://doi.org/10.1038/s41598-021-91280-6.
[22] S.S. Masoud, A. Kovacevich, R. Gangji, H. Nyawale, M. Nyange, A. Ntukula, Extent and resistance patterns of ESKAPE pathogens isolated in pus swabs from hospitalized patients, Can. J. Infect. Dis. Med. Microbiol. 2022 (2022) 3511306, https://doi.org/10.1155/2022/3511306.
[23] A. Singh, A.N. Singh, N. Rathor, R. Chaudhry, S.K. Singh, G. Nath, Evaluation of bacteriophage cocktail on septicemia caused by colistin-resistant *Klebsiella pneumoniae* in mice model, Front. Pharmacol. 13 (2022), 778676, https://doi.org/10.3389/fphar.2022.778676.
[24] P. Hyman, Phages for phage therapy: isolation, characterization, and host range breadth, Pharmaceuticals (Basel, Switzerland) 12 (1) (2019), https://doi.org/10.3390/ph12010035.
[25] T. Luong, A.C. Salabarria, R.A. Edwards, D.R. Roach, Standardized bacteriophage purification for personalized phage therapy, Nat. Protoc. 15 (9) (2020) 2867–2890, https://doi.org/10.1038/s41596-020-0346-0.
[26] A.M. Kropinski, A. Mazzocco, T.E. Waddell, E. Lingohr, R.P. Johnson, Enumeration of bacteriophages by double agar overlay plaque assay, Methods Mol. Biol. (Clifton, N.J.) 501 (2009) 69–76, https://doi.org/10.1007/978-1-60327-164-6_7.
[27] D.M. El-Atrees, R.F. El-Kased, A.M. Abbas, M.A. Yassien, Characterization and anti-biofilm activity of bacteriophages against urinary tract Enterococcus faecalis isolates, Sci. Rep. 12 (1) (2022) 13048, https://doi.org/10.1038/s41598-022-17275-z.
[28] A. Jurczak-Kurek, T. Gąsior, B. Nejman-Faleńczyk, S. Bloch, A. Dydecka, G. Topka, A. Necel, M. Jakubowska-Deredas, M. Narajczyk, M. Richert, A. Mieszkowska, B. Wróbel, G. Węgrzyn, A. Węgrzyn, Biodiversity of bacteriophages: morphological and biological properties of a large group of phages isolated from urban sewage, Sci. Rep. 6 (1) (2016) 34338, https://doi.org/10.1038/srep34338.
[29] A. Singh, A.N. Singh, N. Rathor, R. Chaudhry, S.K. Singh, G. Nath, Evaluation of bacteriophage cocktail on septicemia caused by colistin-resistant klebsiella pneumoniae in mice model, Front. Pharmacol. 13 (2022), https://doi.org/10.3389/fphar.2022.778676.
[30] M. Askoura, N. Saed, G. Enan, A. Askora, Characterization of polyvalent bacteriophages targeting multidrug-resistant Klebsiella pneumonia with enhanced anti-biofilm activity, Appl. Biochem. Microbiol. 57 (1) (2021) 117–126, https://doi.org/10.1134/S000368382101004X.
[31] W. Zhou, Y. Feng, Z. Zong, Two new lytic bacteriophages of the myoviridae family against carbapenem-resistant Acinetobacter baumannii 9 (2018), https://doi.org/10.3389/fmicb.2018.00850.
[32] E.L. Ellis, M. Delbruck, The growth of bacteriophage, J. Gen. Physiol. 22 (3) (1939) 365–384.
[33] Y. Chang, H. Shin, J.H. Lee, C.J. Park, S.Y. Paik, S. Ryu, Isolation and genome characterization of the virulent *Staphylococcus aureus* Bacteriophage SA97, Viruses 7 (10) (2015) 5225–5242, https://doi.org/10.3390/v7102870.
[34] J.K. Akhwale, M. Rohde, C. Rohde, B. Bunk, C. Spröer, H.I. Boga, H.P. Klenk, J. Wittmann, Isolation, characterization and analysis of bacteriophages from the haloalkaline lake Elmenteita, Kenya, PloS one 14 (4) (2019), e0215734, https://doi.org/10.1371/journal.pone.0215734.
[35] A. Allué-Guardia, J. Jofre, M. Muniesa, Stability and infectivity of cytolethal distending toxin type V gene-carrying bacteriophages in a water mesocosm and under different inactivation conditions, Appl. Environ. Microbiol. 78 (16) (2012) 5818–5823, https://doi.org/10.1128/aem.00997-12.
[36] E. Vitzilaiou, Y. Liang, J.L. Castro-Mejía, C.M.A.P. Franz, H. Neve, F.K. Vogensen, S. Knøchel, UV tolerance of Lactococcus lactis 936-type phages: impact of wavelength, matrix, and pH, Int. J. Food Microbiol. 378 (2022) 109824, https://doi.org/10.1016/j.ijfoodmicro.2022.109824.

[37] Y. Pan, X. Ren, S. Wang, X. Li, X. Luo, Z. Yin, Annexin V-conjugated mixed micelles as a potential drug delivery system for targeted thrombolysis, Biomacromolecules 18 (3) (2017) 865–876, https://doi.org/10.1021/acs.biomac.6b01756.

[38] R. Sareen, M. Kapil, G.N. Gupta, Incubation and its effect on Leishman stain, J. Lab. Physicians 10 (3) (2018) 357–361, https://doi.org/10.4103/jlp.Jlp_154_17.

[39] M.P. MacWilliams, M.K. Liao, Luria broth (LB) and Luria agar (LA) media and their uses protocol, J ASM 2006 (2006).

[40] D. Dehari, A.K. Mehata, V. Priya, D. Parbat, D. Kumar, A.K. Srivastava, S. Singh, A.K. Agrawal, Luliconazole nail lacquer for the treatment of onychomycosis: formulation, characterization and in vitro and ex vivo evaluation, AAPS PharmSciTech 23 (6) (2022) 175, https://doi.org/10.1208/s12249-022-02324-7.

[41] M.O. Ilomuanya, N.V. Enwuru, E. Adenokun, A. Fatunmbi, A. Adeluola, C. I. Igwilo, Chitosan-based microparticle encapsulated *Acinetobacter baumannii* phage cocktail in hydrogel matrix for the management of multidrug resistant chronic wound infection, Turk. J. Pharm. Sci. 19 (2) (2022) 187–195, https://doi.org/10.4274/tjps.galenos.2021.72547.

[42] S. Baghel, V.S. Nair, A. Pirani, A.B. Sravani, B. Bhemisetty, K. Ananthamurthy, J. M. Aranjani, S.A. Lewis, Luliconazole-loaded nanostructured lipid carriers for topical treatment of superficial Tinea infections, Dermatol. Ther. 33 (6) (2020), e13959, https://doi.org/10.1111/dth.13959.

[43] X. Li, X. Kong, S. Shi, X. Zheng, G. Guo, Y. Wei, Z. Qian, Preparation of alginate coated chitosan microparticles for vaccine delivery, BMC Biotechnol. 8 (1) (2008) 89, https://doi.org/10.1186/1472-6750-8-89.

[44] M.M. Anjum, K.K. Patel, D. Dehari, N. Pandey, R. Tilak, A.K. Agrawal, S. Singh, Anacardic acid encapsulated solid lipid nanoparticles for Staphylococcus aureus biofilm therapy: chitosan and DNase coating improves antimicrobial activity, Drug Deliv. Transl. Res. 11 (1) (2021) 305–317, https://doi.org/10.1007/s13346-020-00795-4.

[45] S. Proniuk, J. Blanchard, Anhydrous Carbopol® polymer gels for the topical delivery of oxygen/water sensitive compounds, Pharm. Dev. Technol. 7 (2) (2002) 249–255, https://doi.org/10.1081/PDT-120003492.

[46] M.G.B. Dantas, S.A.G.B. Reis, C.M.D. Damasceno, L.A. Rolim, P.J. Rolim-Neto, F. O. Carvalho, L.J. Quintans-Junior, J.R.G.d.S. Almeida, Development and evaluation of stability of a gel formulation containing the monoterpene borneol, Sci. World J. 2016 (2016), https://doi.org/10.1155/2016/7394685.

[47] K.K. Patel, D.B. Surekha, M. Tripathi, M.M. Anjum, M.S. Muthu, R. Tilak, A. K. Agrawal, S. Singh, Antibiofilm potential of silver sulfadiazine-loaded nanoparticle formulations: a study on the effect of dnase-i on microbial biofilm and wound healing activity, Mol. Pharm. 16 (9) (2019) 3916–3925, https://doi.org/10.1021/acs.molpharmaceut.9b00527.

[48] Y. Zhang, M. Huo, J. Zhou, A. Zou, W. Li, C. Yao, S. Xie, DDSolver: an add-in program for modeling and comparison of drug dissolution profiles, AAPS J. 12 (3) (2010) 263–271, https://doi.org/10.1208/s12248-010-9185-1.

[49] H. Choudhary, A. Agrawal, R. Malviya, S. Yadav, Y. Jaliwala, U. Patil, Evaluation and optimization of preparative variables for controlled-release floating microspheres of levodopa/carbidopa, J. Die Pharmazie 65 (3) (2010) 194–198.

[50] C. Rodríguez-Melcón, C. Alonso-Calleja, C. García-Fernández, J. Carballo, R. Capita, Minimum Inhibitory Concentration (MIC) and Minimum Bactericidal Concentration (MBC) for twelve antimicrobials (biocides and antibiotics) in eight strains of listeria monocytogenes, Biology 11 (1) (2021) 46, https://doi.org/10.3390/biology11010046.

[51] M. Plota, E. Sazakli, N. Giormezis, F. Gkartziou, F. Kolonitsiou, M. Leotsinidis, S. G. Antimisiaris, I. Spiliopoulou, In vitro anti-biofilm activity of bacteriophage K (ATCC 19685-B1) and Daptomycin against Staphylococci, Microorganisms 9 (9) (2021), https://doi.org/10.3390/microorganisms9091853.

[52] Y. Liu, P. She, L. Xu, L. Chen, Y. Li, S. Liu, Z. Li, Z. Hussain, Y. Wu, Antimicrobial, antibiofilm, and anti-persister activities of penfluridol against *Staphylococcus aureus*, Front. Microbiol. 12 (2021), 727692, https://doi.org/10.3389/fmicb.2021.727692.

[53] X. Guo, S. Liu, X. Zhou, H. Hu, K. Zhang, X. Du, X. Peng, B. Ren, L. Cheng, M. Li, Effect of D-cysteine on dual-species biofilms of Streptococcus mutans and Streptococcus sanguinis, Sci. Rep. 9 (1) (2019) 6689, https://doi.org/10.1038/s41598-019-43081-1.

[54] L.C. Gomes, F.J. Mergulhao, SEM analysis of surface impact on biofilm antibiotic treatment, Scanning 2017 (2017) 2960194, https://doi.org/10.1155/2017/2960194.

[55] D. Li, P. Li, J. Zang, J. Liu, Enhanced hemostatic performance of tranexamic acid-loaded chitosan/alginate composite microparticles, J. Biotechnol. Biomed. 2012 (2012), 981321, https://doi.org/10.1155/2012/981321.

[56] L. Elias, R. Taengua, B. Frígols, B. Salesa, Á. Serrano-Aroca, Carbon nanomaterials and LED irradiation as antibacterial strategies against Gram-positive multidrug-resistant pathogens, Int. J. Mol. Sci. 20 (14) (2019) 3603, https://doi.org/10.3390/ijms20143603.

[57] T. Kim, Q. Zhang, J. Li, L. Zhang, J.V. Jokerst, A gold/silver hybrid nanoparticle for treatment and photoacoustic imaging of bacterial infection, ACS Nano 12 (6) (2018) 5615–5625, https://doi.org/10.1021/acsnano.8b01362.

[58] T. Suda, T. Hanawa, M. Tanaka, Y. Tanji, K. Miyanaga, S. Hasegawa-Ishii, K. Shirato, T. Kizaki, T. Matsuda, Modification of the immune response by bacteriophages alters methicillin-resistant *Staphylococcus aureus* infection, Sci. Rep. 12 (1) (2022) 15656, https://doi.org/10.1038/s41598-022-19922-x.

[59] U. Puapermpoonsiri, J. Spencer, C.F. van der Walle, A freeze-dried formulation of bacteriophage encapsulated in biodegradable microspheres, Eur. J. Pharm. Biopharm. 72 (1) (2009) 26–33, https://doi.org/10.1016/j.ejpb.2008.12.001.

[60] R. Serra, R. Grande, L. Butrico, A. Rossi, U.F. Settimio, B. Caroleo, B. Amato, L. Gallelli, S. de Franciscis, Chronic wound infections: the role of *Pseudomonas aeruginosa* and *Staphylococcus aureus*, Expert Rev. Anti Infect. Ther. 13 (5) (2015) 605–613, https://doi.org/10.1586/14787210.2015.1023291.

[61] F. Teng, X. Xiong, S. Zhang, G. Li, R. Wang, L. Zhang, X. Wang, H. Zhou, J. Li, Y. Li, Y. Jiang, W. Cui, L. Tang, L. Wang, X. Qiao, Efficacy assessment of phage therapy in treating *Staphylococcus aureus*-induced mastitis in mice, Viruses 14 (3) (2022) 620, https://doi.org/10.3390/v14030620.

[62] S. Sharma, S. Datta, S. Chatterjee, M. Dutta, J. Samanta, M.G. Vairale, R. Gupta, V. Veer, S.K. Dwivedi, Isolation and characterization of a lytic bacteriophage against Pseudomonas aeruginosa, Sci. Rep. 11 (1) (2021) 19393, https://doi.org/10.1038/s41598-021-98457-z.

[63] S. Kaur, A. Kumari, A. Kumari Negi, V. Galav, S. Thakur, M. Agrawal, V. Sharma, Nanotechnology based approaches in phage therapy: overcoming the pharmacological barriers, Front. Pharmacol. 12 (2021) 699054, https://doi.org/10.3389/fphar.2021.699054.

[64] N. Ramesh, L. Archana, M. Madurantakam Royam, P. Manohar, K. Eniyan, Effect of various bacteriological media on the plaque morphology of Staphylococcus and Vibrio phages, Access Microbiol 1 (4) (2019) 36, https://doi.org/10.1099/acmi.0.000036.

[65] B.S. Gudlavalleti, T. Phung, C.L. Barton, A. Becker, B.L. Graul, J.T. Griffin, C. J. Hays, B. Horn, D.R. Liang, L.M. Rutledge, A.M. Szalanczy, B.L. Gaffney, R. A. King, C.A. Rinehart, A.K. Staples, A.A. Stewart, M.L. Nydam, K.E. O'Quin, Whole genome sequencing identifies an allele responsible for clear vs. turbid plaque morphology in a Mycobacteriophage, BMC Microbiol. 20 (1) (2020) 148, https://doi.org/10.1186/s12866-020-01833-4.

[66] A. Ross, S. Ward, P. Hyman, More is better: selecting for broad host range bacteriophages, Front. Microbiol. 7 (2016) 1352, https://doi.org/10.3389/fmicb.2016.01352.

[67] P. Hyman, S.T. Abedon, Bacteriophage host range and bacterial resistance, J. Adv. Appl. Microbiol. 70 (2010) 217–248.

[68] V. Abatángelo, N. Peressutti Bacci, C.A. Boncompain, A.F. Amadio, S. Carrasco, C. A. Suárez, H.R. Morbidoni, Broad-range lytic bacteriophages that kill Staphylococcus aureus local field strains, PloS one 12 (7) (2017), e0181671, https://doi.org/10.1371/journal.pone.0181671.

[69] M. Rahman, S. Kim, S.M. Kim, S.Y. Seol, J. Kim, Characterization of induced Staphylococcus aureus bacteriophage SAP-26 and its anti-biofilm activity with rifampicin, Biofouling 27 (10) (2011) 1087–1093, https://doi.org/10.1080/08927014.2011.631169.

[70] M. Imam, B. Alrashid, F. Patel, A.S.A. Dowah, N. Brown, A. Millard, M.R. J. Clokie, E.E. Galyov, vB_PaeM_MIJ3, a novel jumbo phage infecting *Pseudomonas aeruginosa*, possesses unusual genomic features, Front. Microbiol. (2019) 2772.

[71] J.E. Han, J.H. Kim, S.Y. Hwang, C.H. Choresca Jr., S.P. Shin, J.W. Jun, J.Y. Chai, Y.H. Park, S.C. Park, Isolation and characterization of a Myoviridae bacteriophage against Staphylococcus aureus isolated from dairy cows with mastitis, Res. Vet. Sci. 95 (2) (2013) 758–763, https://doi.org/10.1016/j.rvsc.2013.06.001.

[72] A. Hamza, S. Perveen, Z. Abbas, S.U. Rehman, The lytic SA phage demonstrate bactericidal activity against mastitis causing Staphylococcus aureus 11 (1) (2016) 39–45, https://doi.org/10.1515/biol-2016-0005.

[73] I. Titze, T. Lehnherr, H. Lehnherr, V. Krömker, Efficacy of bacteriophages against staphylococcus aureus isolates from Bovine Mastitis 13 (3) (2020) 35.

[74] F. Mohammadian, H.K. Rahmani, B. Bidarian, B. Khoramian, Isolation and evaluation of the efficacy of bacteriophages against multidrug-resistant (MDR), methicillin-resistant (MRSA) and biofilm-producing strains of Staphylococcus aureus recovered from bovine mastitis, BMC Vet. Res. 18 (1) (2022) 406, https://doi.org/10.1186/s12917-022-03501-3.

[75] Y.Y. Feng, S.L. Ong, J.Y. Hu, X.L. Tan, W.J. Ng, Effects of pH and temperature on the survival of coliphages MS2 and Qbeta, J. Ind. Microbiol. Biotechnol. 30 (9) (2003) 549–552, https://doi.org/10.1007/s10295-003-0080-y.

[76] E. Jończyk, M. Kłak, R. Międzybrodzki, A. Górski, The influence of external factors on bacteriophages—review, Folia Microbiol. 56 (3) (2011) 191–200, https://doi.org/10.1007/s12223-011-0039-8.

[77] A. Pradeep, S. Ramasamy, J. Veniemilda, C.V. Kumar, Effect of pH & temperature variations on phage stability - a crucial prerequisite for successful phage therapy, IJPSR 13 (12) (2022) 5178–5182.

[78] B. Pallavi, T.G. Puneeth, M. Shekar, S.K. Girisha, Isolation, characterization and genomic analysis of vB-AhyM-AP1, a lytic bacteriophage infecting *Aeromonas hydrophila*, J. Appl. Microbiol. 131 (2) (2021) 695–705, https://doi.org/10.1111/jam.14997.

[79] K. Ramirez, C. Cazarez-Montoya, H.S. Lopez-Moreno, N. Castro-Del Campo, Bacteriophage cocktail for biocontrol of *Escherichia coli* O157:H7: stability and potential allergenicity study, PloS one 13 (5) (2018), e0195023, https://doi.org/10.1371/journal.pone.0195023.

[80] Y. Ma, J.C. Pacan, Q. Wang, Y. Xu, X. Huang, A. Korenevsky, P.M. Sabour, Microencapsulation of bacteriophage felix O1 into chitosan-alginate microspheres for oral delivery, Appl. Environ. Microbiol. 74 (15) (2008) 4799–4805, https://doi.org/10.1128/aem.00246-08.

[81] S. Kim, A. Jo, F.S. Ahn, Technology, application of chitosan–alginate microspheres for the sustained release of bacteriophage in simulated gastrointestinal conditions 50 (4) (2015) 913–918.

[82] R. Jamaledin, R. Sartorius, C. Di Natale, V. Onesto, R. Manco, V. Mollo, R. Vecchione, P. De Berardinis, P.A. Netti, PLGA microparticle formulations for tunable delivery of a nano-engineered filamentous bacteriophage-based vaccine:

in vitro and in silico-supported approach, J. Nanostructure Chem. (2023), https://doi.org/10.1007/s40097-022-00519-9.
[83] P.P. Kalelkar, D.A. Moustafa, M. Riddick, J.B. Goldberg, N.A. McCarty, A. J. García, Bacteriophage-loaded poly(lactic-co-glycolic acid) microparticles mitigate staphylococcus aureus infection and cocultures of *Staphylococcus aureus* and *Pseudomonas aeruginosa*, Adv. Healthc. Mater. 11 (10) (2022), e2102539, https://doi.org/10.1002/adhm.202102539.
[84] A.F. Martins, D.M. de Oliveira, A.G.B. Pereira, A.F. Rubira, E.C. Muniz, Chitosan/TPP microparticles obtained by microemulsion method applied in controlled release of heparin, Int. J. Biol. Macromol. 51 (5) (2012) 1127–1133, https://doi.org/10.1016/j.ijbiomac.2012.08.032.
[85] S. Sreekumar, F.M. Goycoolea, B.M. Moerschbacher, G.R. Rivera-Rodriguez, Parameters influencing the size of chitosan-TPP nano- and microparticles, Sci. Rep. 8 (1) (2018) 4695, https://doi.org/10.1038/s41598-018-23064-4.
[86] P.K. Montso, V. Mlambo, C.N. Ateba, Characterization of lytic bacteriophages infecting multidrug-resistant shiga toxigenic atypical *Escherichia coli* O177 strains isolated from cattle feces, Front. Public Health 7 (2019) 355, https://doi.org/10.3389/fpubh.2019.00355.
[87] M.M. D'Andrea, D. Frezza, E. Romano, P. Marmo, L.H. De Angelis, N. Perini, M. C. Thaller, G. Di Lallo, The lytic bacteriophage vB_EfaH_EF1TV, a new member of the Herelleviridae family, disrupts biofilm produced by enterococcus faecalis clinical strains, J. Glob. Antimicrob. Resist. 21 (2020) 68–75.
[88] R. Armon, Y. Kott, A simple, rapid and sensitive presence/absence detection test for bacteriophage in drinking water, J. Appl. Bacteriol. 74 (4) (1993) 490–496.
[89] J. Woolston, A.R. Parks, T. Abuladze, B. Anderson, M. Li, C. Carter, L.F. Hanna, S. Heyse, D. Charbonneau, A. Sulakvelidze, Bacteriophages lytic for Salmonella rapidly reduce Salmonella contamination on glass and stainless steel surfaces, Bacteriophage 3 (3) (2013), e25697.
[90] A.K. Seth, M.R. Geringer, K.T. Nguyen, S.P. Agnew, Z. Dumanian, R.D. Galiano, K. P. Leung, T.A. Mustoe, S.J. Hong, Bacteriophage therapy for *Staphylococcus aureus* biofilm-infected wounds: a new approach to chronic wound care, Plast. Reconst. Surg. 131 (2) (2013) 225–234, https://doi.org/10.1097/PRS.0b013e31827e47cd.
[91] S. Kumari, K. Harjai, S. Chhibber, Bacteriophage versus antimicrobial agents for the treatment of murine burn wound infection caused by Klebsiella pneumoniae B5055, J. Med. Microbiol. 60 (Pt 2) (2011) 205–210, https://doi.org/10.1099/jmm.0.018580-0.
[92] J. Luo, L. Xie, M. Liu, Q. Li, P. Wang, C. Luo, Bactericidal synergism between phage YC#06 and antibiotics: a combination strategy to target multidrug-resistant acinetobacter baumannii in vitro and in vivo, Microbiol. Spectr. 10 (4) (2022), e0009622, https://doi.org/10.1128/spectrum.00096-22.
[93] F.L. Short, S.L. Murdoch, R.P. Ryan, Polybacterial human disease: the ills of social networking, Trends Microbiol. 22 (9) (2014) 508–516, https://doi.org/10.1016/j.tim.2014.05.007.
[94] Z. Chegini, A. Khoshbayan, M. Taati Moghadam, I. Farahani, P. Jazireian, A. Shariati, Bacteriophage therapy against *Pseudomonas aeruginosa* biofilms: a review, Ann. Clin. Microbiol. Antimicrob. 19 (1) (2020) 45, https://doi.org/10.1186/s12941-020-00389-5.
[95] S. Amankwah, K. Abdella, T. Kassa, Bacterial biofilm destruction: a focused review on the recent use of phage-based strategies with other antibiofilm agents, Nanotechnol. Sci. Appl. 14 (2021) 161–177, https://doi.org/10.2147/nsa.S325594.
[96] A. Cevallos-Urena, J.Y. Kim, B.S. Kim, Vibrio-infecting bacteriophages and their potential to control biofilm, Food Sci. Biotechnol. 32 (2023) 1719–1727, https://doi.org/10.1007/s10068-023-01361-7.
[97] P. Rivera Aguayo, T. Bruna Larenas, C. Alarcón Godoy, B. Cayupe Rivas, J. González-Casanova, D. Rojas-Gómez, N. Caro Fuentes, Antimicrobial and antibiofilm capacity of chitosan nanoparticles against wild type strain of Pseudomonas sp. isolated from milk of cows diagnosed with bovine mastitis, Antibiotics (Basel) 9 (9) (2020) 551, https://doi.org/10.3390/antibiotics9090551.
[98] A.S. Abdelsattar, A.Y. Yakoup, Y. Khaled, A. Safwat, A. El-Shibiny, The synergistic effect of using bacteriophages and chitosan nanoparticles against pathogenic bacteria as a novel therapeutic approach, Int. J. Biol. Macromol. 228 (2023) 374–384, https://doi.org/10.1016/j.ijbiomac.2022.12.246.
[99] M. Adnan, M.R. Ali Shah, M. Jamal, F. Jalil, S. Andleeb, M.A. Nawaz, S. Pervez, T. Hussain, I. Shah, M. Imran, A. Kamil, Isolation and characterization of bacteriophage to control multidrug-resistant Pseudomonas aeruginosa planktonic cells and biofilm, Biologicals 63 (2020) 89–96, https://doi.org/10.1016/j.biologicals.2019.10.003.
[100] C. de la Fuente-Núñez, F. Reffuveille, L. Fernández, R.E. Hancock, Bacterial biofilm development as a multicellular adaptation: antibiotic resistance and new therapeutic strategies, Curr. Opin. Microbiol. 16 (5) (2013) 580–589, https://doi.org/10.1016/j.mib.2013.06.013.
[101] A.C. Duarte, L. Fernández, V. De Maesschalck, D. Gutiérrez, A.B. Campelo, Y. Briers, R. Lavigne, A. Rodríguez, P. García, Synergistic action of phage phiIPLA-RODI and lytic protein CHAPSH3b: a combination strategy to target *Staphylococcus aureus* biofilms, NPJ Biofilms Microbiomes 7 (1) (2021) 39, https://doi.org/10.1038/s41522-021-00208-5.
[102] L.C. Powell, M.F. Pritchard, E.L. Ferguson, K.A. Powell, S.U. Patel, P.D. Rye, S.-M. Sakellakou, N.J. Buurma, C.D. Brilliant, J.M. Copping, G.E. Menzies, P. D. Lewis, K.E. Hill, D.W. Thomas, Targeted disruption of the extracellular polymeric network of *Pseudomonas aeruginosa* biofilms by alginate oligosaccharides, NPJ Biofilms Microbiomes 4 (1) (2018) 13, https://doi.org/10.1038/s41522-018-0056-3.
[103] S. Chatterjee, N. Biswas, A. Datta, R. Dey, P. Maiti, Atomic force microscopy in biofilm study, Microscopy (Oxford, England) 63 (4) (2014) 269–278, https://doi.org/10.1093/jmicro/dfu013.
[104] G. Donelli, C. Vuotto, Biofilm-based infections in long-term care facilities, Future microbiology 9 (2) (2014) 175–188, https://doi.org/10.2217/fmb.13.149.
[105] M.A. Ansari, H.M. Khan, A.A. Khan, S.S. Cameotra, R. Pal, Antibiofilm efficacy of silver nanoparticles against biofilm of extended spectrum β-lactamase isolates of *Escherichia coli* and *Klebsiella pneumoniae*, Appl. Nanosci. 4 (7) (2014) 859–868, https://doi.org/10.1007/s13204-013-0266-1.
[106] K. Kosznik-Kwaśnicka, M. Stasiłojć, G. Stasiłojć, N. Kaźmierczak, L. Piechowicz, The influence of bacteriophages on the metabolic condition of human fibroblasts in light of the safety of phage therapy in staphylococcal skin infections 24 (6) (2023) 5961.
[107] J. Shan, A. Ramachandran, A.M. Thanki, F.B.I. Vukusic, J. Barylski, M.R.J. Clokie, Bacteriophages are more virulent to bacteria with human cells than they are in bacterial culture; insights from HT-29 cells, Sci. Rep. 8 (1) (2018) 5091, https://doi.org/10.1038/s41598-018-23418-y.
[108] L. Rahimzadeh Torabi, M. Doudi, N.S. Naghavi, R. Monajemi, Bacteriophages PΦEn-CL and PΦEn-HO can eliminate MDR Enterobacter cloacae and Enterobacter hormaechei isolated from burn wound infections without toxicity for human skin cells, FEMS Microbiol. Lett. 368 (20) (2021), https://doi.org/10.1093/femsle/fnab143.
[109] K. Petsong, S. Benjakul, K. Vongkamjan, Optimization of wall material for phage encapsulation via freeze-drying and antimicrobial efficacy of microencapsulated phage against Salmonella, J. Food Sci. Technol. 58 (5) (2021) 1937–1946, https://doi.org/10.1007/s13197-020-04705-x.
[110] M. Wdowiak, J. Paczesny, S. Raza, Enhancing the stability of bacteriophages using physical, chemical, and nano-based approaches: a review, Pharmaceutics 14 (9) (2022) 1936, https://doi.org/10.3390/pharmaceutics14091936.
[111] R. Brogna, H. Oldenhof, H. Sieme, C. Figueiredo, T. Kerrinnes, W.F. Wolkers, Increasing storage stability of freeze-dried plasma using trehalose, PloS one 15 (6) (2020), e0234502, https://doi.org/10.1371/journal.pone.0234502.
[112] V. Leung, L. Groves, A. Szewczyk, Z. Hosseinidoust, C.D.M. Filipe, Long-term antimicrobial activity of phage–sugar glasses is closely tied to the processing conditions, ACS Omega 3 (12) (2018) 18295–18303, https://doi.org/10.1021/acsomega.8b02679.
[113] N. Rezk, A.S. Abdelsattar, D. Elzoghby, M.M. Agwa, M. Abdelmoteleb, R.G. Aly, M.S. Fayez, K. Essam, B.M. Zaki, A. El-Shibiny, Bacteriophage as a potential therapy to control antibiotic-resistant Pseudomonas aeruginosa infection through topical application onto a full-thickness wound in a rat model, J. Genet. Eng. Biotechnol. 20 (1) (2022) 133, https://doi.org/10.1186/s43141-022-00409-1.
[114] X. Lin, Y. Shen, L. Wang, Multi-scale photoacoustic assessment of wound healing using chitosan–graphene oxide hemostatic sponge 11 (11) (2021) 2879.
[115] Y. Mantri, J. Tsujimoto, B. Donovan, C.C. Fernandes, P.S. Garimella, W.F. Penny, C.A. Anderson, J.V. Jokerst, Photoacoustic monitoring of angiogenesis predicts response to therapy in healing wounds, Wound Repair Regen. 30 (2) (2022) 258–267, https://doi.org/10.1111/wrr.12992.
[116] M. Puthia, M. Butrym, J. Petrlova, A.C. Strömdahl, M. Andersson, S. Kjellström, A. Schmidtchen, A dual-action peptide-containing hydrogel targets wound infection and inflammation, Sci. Transl. Med. 12 (524) (2020) 6601, https://doi.org/10.1126/scitranslmed.aax6601.
[117] E. Pelfrene, E. Willebrand, A. Cavaleiro Sanches, Z. Sebris, M. Cavaleri, Bacteriophage therapy: a regulatory perspective, J. Antimicrob. Chemother. 71 (8) (2016) 2071–2074, https://doi.org/10.1093/jac/dkw083.